PERGAMON

Journal of Structural Geology 24 (2002) 1903–1924

JOURNAL OF STRUCTURAL GEOLOGY

www.elsevier.com/locate/jstrugeo

Growth, linkage, and termination processes of a 10-km-long strike-slip fault in jointed granite: the Gemini fault zone, Sierra Nevada, California

Matthew A. Pachell[1], James P. Evans*

Department of Geology, Utah State University, Logan, UT 84322-4505, USA

Received 21 December 2000; received in revised form 3 December 2001; accepted 5 February 2002

Abstract

Field-based structural analysis of an exhumed, ~10-km-long strike-slip fault zone elucidates processes of growth, linkage, and termination along moderately sized strike-slip fault zones in granitic rocks. The Gemini fault zone is a 9.3-km-long, left-lateral fault system that was active at depths of 8–11 km within the transpressive Late-Cretaceous Sierran magmatic arc. The fault zone cuts four granitic plutons and is composed of three steeply dipping northeast- and southwest-striking noncoplanar segments that nucleated and grew along preexisting cooling joints. The fault core is bounded by subparallel fault planes that separate highly fractured epidote-, chlorite-, and quartz-breccias from undeformed protolith. The slip profile along the Gemini fault zone shows that the fault zone consists of three 2–3-km-long segments separated by two 'zones' of local slip minima. Slip is highest (131 m) on the western third of the fault zone and tapers to zero at the eastern termination. Slip vectors plunge shallowly west-southwest and show significant variability along strike and across segment boundaries. Four types of microstructures reflect compositional changes in protolith along strike and show that deformation was concentrated on narrow slip surfaces at, or below, greenschist facies conditions. Taken together, we interpret the fault zone to be a segmented, linked fault zone in which geometrical complexities of the faults and compositional variations of protolith and fault rock resulted in nonuniform slip orientations, complex fault-segment interactions, and asymmetric slip-distance profiles. © 2002 Published by Elsevier Science Ltd.

Keywords: Fault growth; Fault structure; Faulting; Strike-slip faulting

1. Introduction

Field-based structural analyses of exhumed fault zones can be used to constrain seismological models of fault zone structure, composition, and deformational processes. Current questions in earthquake seismology that can be partially addressed by field-based geologic investigations include the following:

1. Why, in some cases, do segment boundaries retard rupture propagation and enhance it in others (e.g. Wesnousky, 1986; Beroza and Spudich, 1988; Harris and Day, 1993, 1999)?
2. During an earthquake, slip appears to be concentrated in small 'patches' (Wald et al., 1991; Rubin et al., 1999). What effects do lateral changes in fault zone composition have on the distribution of slip patches along a fault zone (e.g. Chiarabba and Amato, 1994)?
3. What is the relationship between irregular fault geometries and stress variations along a fault zone (e.g. Guatteri and Spudich, 1998)?
4. How do the resulting stress conditions affect slip vectors (e.g. Spudich et al., 1998)? Is this tied to the lateral composition of the fault zone (e.g. Beroza, 1991; Chiarabba and Amato, 1994; Harris and Day, 1997)?

We address these questions by examining the geometry, linkage, termination, slip, and microstructures from the exhumed Gemini fault zone (Martel, 1990), a 9.3-km-long, left-lateral strike-slip fault zone in the east-central Sierra Nevada, California. Our observations, recorded at various stations with a maximum structural relief of ~700 m, is a detailed three-dimensional investigation of 10-km-long, strike-slip fault zone geometry, kinematics, and microstructural composition.

There are numerous studies of 1–100-m-scale (defined here as referring to the trace length of faults) strike-slip faults (e.g. Lockwood and Moore, 1979; Segall and Pollard, 1983a; Martel et al., 1988; Martel and Pollard, 1989; Segall et al., 1990; Martel and Boger, 1998; Robeson, 1998) as well as at the tens to hundreds of kilometers-scale elsewhere (e.g. Sylvester (1988) and references therein). However, few

* Corresponding author. Tel.: +1-435-797-1267; fax: +1-435-797-1588.
E-mail address: jpevans@cc.usu.edu (J.P. Evans).
[1] Now at: Anadarko Petroleum Co., 17701 Northchase, Houston, TX 77060, USA.

0191-8141/02/$ - see front matter © 2002 Published by Elsevier Science Ltd.
PII: S0191-8141(02)00027-5

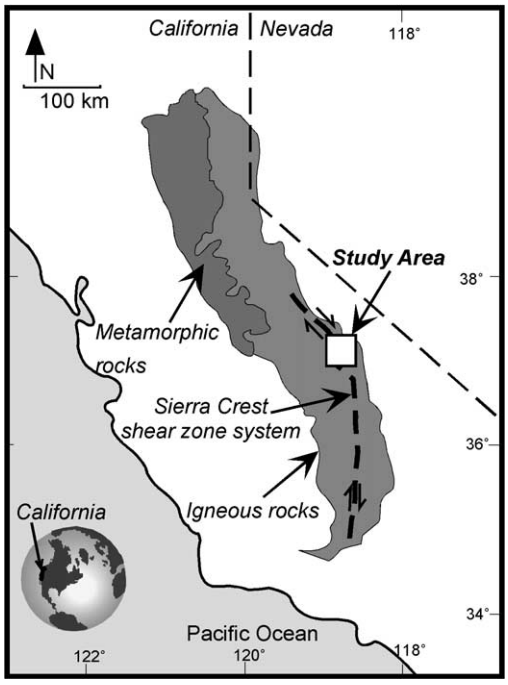

Fig. 1. Location of study area. The study area is in the Mount Abbot quadrangle (Lockwood and Lydon, 1975), between Kings Canyon and Yosemite national parks, California, USA. The location of the Sierra Crest shear zone system is taken from Greene and Schweickert (1995).

studies address the structure of fault zones with trace lengths of 1–10 km. The Gemini fault zone is an exhumed, segmented left-lateral strike-slip fault zone where each segment is 2–3 km long and, if representative of a seismogenic fault at depth, equivalent to a fault capable of producing $M_b = 4$ earthquakes. If the entire 9.3-km-trace length of the fault zone ruptured, it could have produced a $M_b = 5–6$ earthquake (Evans et al., 2000).

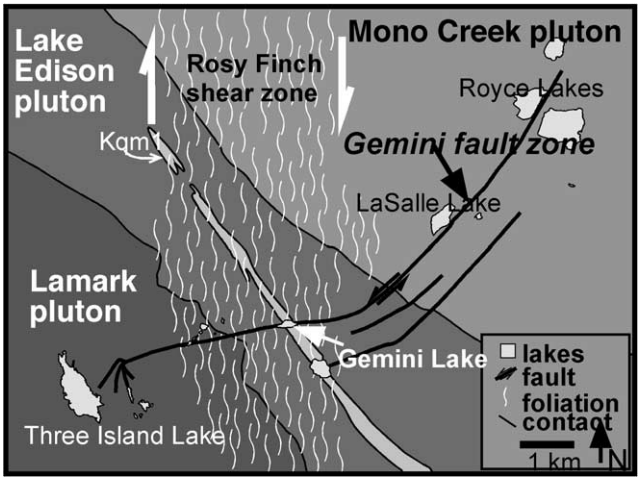

Fig. 2. Generalized geologic map of study area. The Gemini fault zone crosses the Lamark pluton (west), Lake Edison pluton (center), which contains a dike-like body of quartz monzonite (Kqm1, center), and the Mono Creek (east) plutons. The plutons become younger and more felsic to the east. Map modified from Lockwood and Lydon (1975) and Tikoff and Saint Blanquat (1997).

Studies of strike-slip faults at the centimeter- and meter-scale in the Sierra Nevada show that relatively simple fault zones may coalesce into larger compound fault zones that are meters to hundreds of meters in length (e.g. Martel, 1990). One question that has arisen from these studies pertains to fault scaling. Is it possible to apply the observations of meter-scale faults to faults that have trace lengths of several kilometers, as has been done for observations of the surface traces of such faults (e.g. Tchalenko and Abrasey's 1970)? Our data can be directly compared with exhumed meter-scale faults in the same region (e.g. Martel et al., 1988; Martel, 1990), thus the faulting process can be considered over a range of scales in a consistent lithology.

The Gemini fault zone cuts glaciated granitoids, which provide exceptional exposure and limited lithologic heterogeneity. The granitoids are petrographically distinct (Bateman, 1992), but are relatively mechanically homogeneous and overprinted by few post-emplacement deformational events. This makes field-based studies that address fundamental aspects of faulting, such as fault initiation, growth, and termination, less complicated. Furthermore, field-based studies of natural fault systems in granitic rocks augment laboratory experiments and micromechanical models of faulting in granite (e.g. Reches and Lockner, 1994; Moore and Lockner, 1995; Wibberley et al., 2000).

We provide data about the geometry of the fault zone, the magnitude of slip along the fault trace, and mineral lineations and microstructural variations along strike. We discuss the scaling similarities and differences between meter- and 10-km-scale fault geometries for left-lateral strike-slip faults in the study region. We then discuss preexisting structures and their influence on the geometry of the fault zone and suggest that the Gemini fault zone formed and grew along preexisting parallel joints that coalesced via complex linkage zones. Next, we discuss the slip-distance profile in terms of segmentation and slip transfer through segment boundary zones. We conclude with a discussion of the lateral distribution of microstructures and show that narrow slip surfaces form early in the development of the fault zone and are operative on segments regardless of their ultimate slip magnitude.

2. Geologic setting

The granitoids in the study area belong to the John Muir Intrusive Suite, a series of elongate northwest-striking Late Cretaceous plutons that extend southward from Yosemite Valley (Bateman, 1992). These plutons are Late Cretaceous porphyritic granodiorites cut by late-stage aplite dikes (Evernden and Kistler, 1970). These dikes, and the steeply dipping pluton contacts, are critical for the study, as they provide constraints on the net slip across the fault zone. The Gemini fault zone is in the Mount Abbot Quadrangle

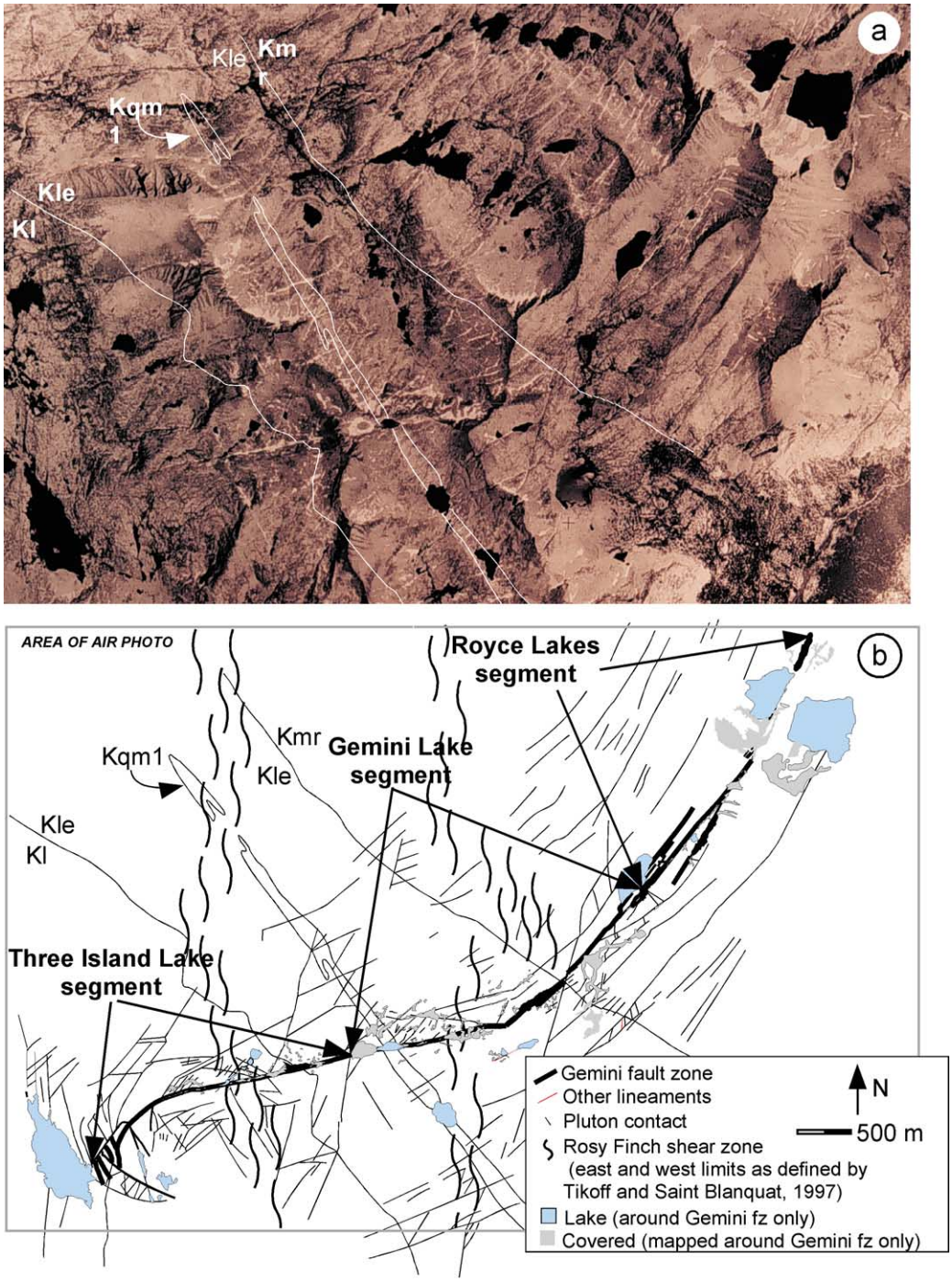

Fig. 3. Aerial photograph (a) and prominent lineations (b) of field area. Segment boundary zones defined by slip minima on distance-displacement plot (Fig. 9). Kl = Lamark granodiorite; Kle = Lake Edison granodiorite; Kqm1 = quartz monzonite/granite (Lockwood and Lydon, 1975).

(Lockwood and Lydon, 1975) of the east-central Sierra Nevada, between Yosemite and Kings Canyon National Parks (Fig. 1). The Gemini fault zone strikes approximately northeast–southwest between Royce Lakes and Three Island Lake in the southwestern quarter of the quadrangle and cuts three plutons (Figs. 2 and 3). The fault cuts the Lamark, Lake Edison, and Mono Creek plutons, and a dike-like body of fine- to medium-grained biotite quartz monzonite and granite in the center of the Lake Edison pluton referred to here by its map symbol, 'Kqm1'.

Several lines of evidence suggest that the left-lateral strike-slip faults in the study area were active at depths of 8–11 km. Amphibole geobarometry shows that crystallization in the Mount Abbot quadrangle is estimated to be between 2 and 3 kb, or 8–11 km (Ague and Brimhall, 1988, their fig. 7) and the plutons cooled through the biotite

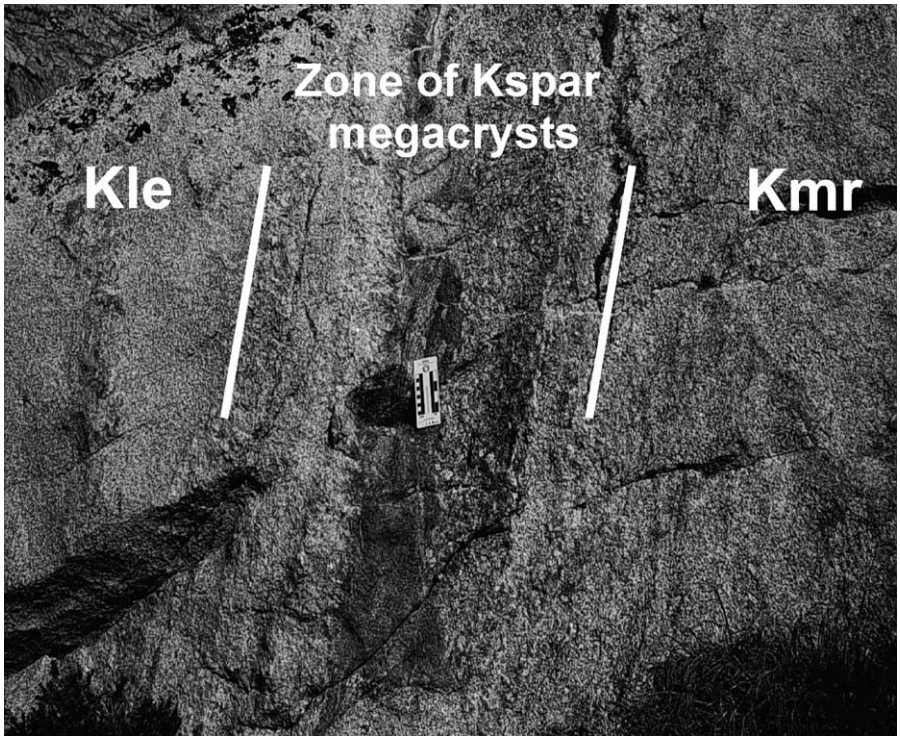

Fig. 4. Lake Edison (Kle) and Mono Creek (Kmr) pluton contact. The contact is defined by a nearly vertical band of feldspar megacrysts. View is to the north along the Gemini fault zone, east of 12221 Peak. The length of the scale card is 16.5 cm.

Ar retention temperature at 85–81 Ma. Segall et al. (1990) dated muscovite from left-lateral strike-slip fault zones near Bear Creek and obtained an age of faulting of 78.9 ± 0.4 Ma (K/Ar and $^{40}Ar/^{39}Ar$ methods). We dated sericite formed in the fault zone at 79.7 ± 0.16 Ma. This age is close to the crystallization age of the Mono Creek pluton. Assuming a geothermal gradient of 30–35 °C/km and the 8–11 km depth estimates of Ague and Brimhall (1988), the Gemini fault zone was likely to have been active at or near the base of the seismogenic zone.

Pluton contacts dip steeply and record slip along the fault zone. Along the Gemini fault zone, the contact between the Lamark granodiorite and the Lake Edison granodiorite dips steeply and is gradational over 3–5 m. In the field it is defined by a 1–3-m-thick band of north–south elongate mafic inclusions that separate a porphyritic facies of the Lamark granodiorite from a finer-grained, slightly more felsic Lake Edison granodiorite. The contact of the Lake Edison granodiorite and Kqm1 dips steeply and sharply juxtaposes the dark-colored Lake Edison granodiorite against the lighter Kqm1. Along the Gemini fault zone, the contact of the Lake Edison granodiorite and the Mono Creek pluton is defined by a narrow (20–70 cm) band of feldspar crystals that dip steeply and juxtapose the dark-colored Lake Edison granodiorite and the lighter Mono Creek pluton (Fig. 4).

The Lamark granodiorite and the Lake Edison granodiorite have a prominent steeply dipping, north-northwest-striking foliation defined by elongate biotite and hornblende crystals and elongate mafic inclusions. The Mono Creek pluton, however, exhibits a weakly defined, steeply dipping, foliation expressed through biotite and hornblende.

All three plutons are cut by aplite and pegmatite dikes that strike dominantly northwest, northeast, and east. They range in thickness from <10 cm to 200 cm and are up to several hundred meters in length. A series of steeply dipping mafic dikes also cuts the Lamark granodiorite. All three types of dikes were used to measure slip along the Gemini fault zone.

3. Preexisting structures in the study area

3.1. The Rosy Finch shear zone

The center of the Gemini fault zone (Fig. 3) cuts subvertical foliation mapped by Lockwood and Lydon (1975) as ‘a zone of pervasive shearing’. Tikoff (1994) interprets the zone to be part of the Rosy Finch shear zone (RFSZ), a Late Cretaceous right-lateral shear zone thought to be related to transpressional tectonics and pluton emplacement along the axis of the Sierra Nevada batholith. Tikoff (1994) and Tikoff and Greene (1994) classify the RFSZ as part of the Sierra Crest shear zone system, a series of late Cretaceous right-lateral shear zones in the eastern Sierra Nevada (Fig. 1). In the study area, the shear zone crosses the Gemini fault zone in the thin neck of the Lake Edison pluton. It is characterized by a broad band of subvertical

northwest-striking mica folia and shallowly plunging lineations defined by elongate quartz grains (Tikoff, 1994; Tikoff and Saint Blanquat, 1997). A possible kinematic relationship between the Rosy Finch shear zone and the Gemini fault zone will be discussed in a companion paper, in which the 83 Ma Rosy Finch Shear zone is cut by the 79 Ma Gemini fault zone during uplift, cooling, and regional right lateral shearing of the area.

3.2. Joints

Numerous studies in the Mount Abbot quadrangle show that ubiquitous joints were reactivated as left-lateral strike-slip fault zones during the waning stage of late Cretaceous magmatism (Lockwood and Moore, 1979; Segall and Pollard, 1983a; Martel et al., 1988; Martel and Pollard, 1989; Segall et al., 1990; Martel and Boger, 1998; Robeson, 1998; Bergbauer and Martel, 1999). Segall and Pollard (1983a) show that joints, filled with chlorite, epidote, sericite, muscovite, calcite and possibly some zeolites, strike northeast, dip steeply southeast, and range in length from millimeters to tens of meters. The ages of the plutons (~86–91 Ma) and the left-lateral faulting (~79 Ma) closely bracket the age of jointing and suggest the joints opened as the plutons cooled. Bergbauer and Martel (1999), through thermo-elastic modeling of the Lake Edison pluton, demonstrate the importance of pluton geometry on the orientation of the cooling joints. Many of the joints were later reactivated to form left-lateral strike-slip fault zones (Martel et al., 1988; Martel, 1990) that range in trace length from meters to several kilometers. Individual fault zones link via splay fractures that strike ~30° counterclockwise to the main fault strand, an orientation that is thought to parallel the maximum compressive stress at the time of faulting (Martel et al., 1988). Martel et al. (1988) show that fault propagation did not result in the generation of new fault-parallel fractures, but was the result of the linkage of individual joints and indicates that the joints control the geometry of the younger faults.

4. Methods

The analyses and interpretation of the geometry and kinematics of the fault zone and joints are based on field observations and mapping on a topographic base and unrectified aerial photographs at a scale of approximately 1:14,000. These data were later transferred to a rectified orthophoto quadrangle at a scale of 1:24,000 (Fig. 3). Steep cirque headwalls were mapped on aerial photos from selected vantage points. Fault strikes and dips are presented using a right-hand rule. The slip-distance analysis was completed by matching dikes, schlieren bands, or pluton contacts that crossed the fault zone at high angles. Slip was calculated using geometric diagrams and lower hemisphere stereonets, which take into account the apparent dip of the dike, pluton contact, or schlieren bands on the fault surface, slip vectors, and topography. The microstructural observations and interpretations are based on analyses of fifty-one 50 mm × 76 mm thin sections cut in two orientations: (1) perpendicular to the fault surface and parallel to slip vector, and (2) perpendicular to both the fault surface and the slip vector.

Microstructural analyses provide insight into internal fault-zone deformational processes, material property variations along fault strike, and fault-zone hydrology, rheology, and evolution. These observations can be used to understand and characterize the occurrence of low- and high-seismic velocity zones (LVZs and HVZs (Ben-Zion, 1998)), which are areas along a fault that are composed of weak materials undergoing aseismic slip and strong materials that exhibit large, coseimic slip (Chiarabba and Amato, 1994). Current studies in earthquake dynamics and prediction indicate that these areas can be identified from local earthquake tomography, but the exact structure and composition of these areas remain unclear (Chiarabba and Amato, 1994; Hough et al., 1994; Harris and Day, 1997). Qualitative microstructural analysis of an exhumed seismogenic strike-slip fault zone provides detailed descriptions of fault zone composition and material properties along fault strike (i.e. LVZs and HVZs), documents the deformation mechanisms active at seismogenic depths, and provides a link between field-based geologic data and seismic analyses.

5. Results

5.1. Geometry and kinematics of meter-scale structures

The curved trace of the Gemini fault zone in the study area is 9.3 km long, trends northeast, and is composed of a linked series of steeply dipping faults (Fig. 2). Commonly the fault is expressed as a snow- or vegetation-filled topographic depression or fault troughs bounded by two parallel faults. Typically the fault trough is 2–15 m wide and 1–15 m deep (Fig. 5a and b). Parallel bounding fault surfaces separate highly fractured chlorite breccias in the trough from undeformed protolith. The trough walls are commonly mineralized with chlorite and epidote and preserve slickenline and slickenside surfaces. Within the trough, the rocks are mostly concealed by vegetation or snow; however, where exposed, they consist of a highly fractured chlorite breccia (Fig. 5c and d). Adjacent to the Gemini fault zone, there are joints and small faults (reactivated joints) that have slickenlines, slickensides, and net slips of ≤1 m. Aerial photographs of the study area show that vegetated or snow-bound troughs, spaced ~0.1–0.5 km apart, are common. If these troughs contain fault zones, the Gemini fault zone may be one of many kilometer-scale fault zones in the region.

The following presentation is divided into three sections that correspond to segments along the fault zone. The

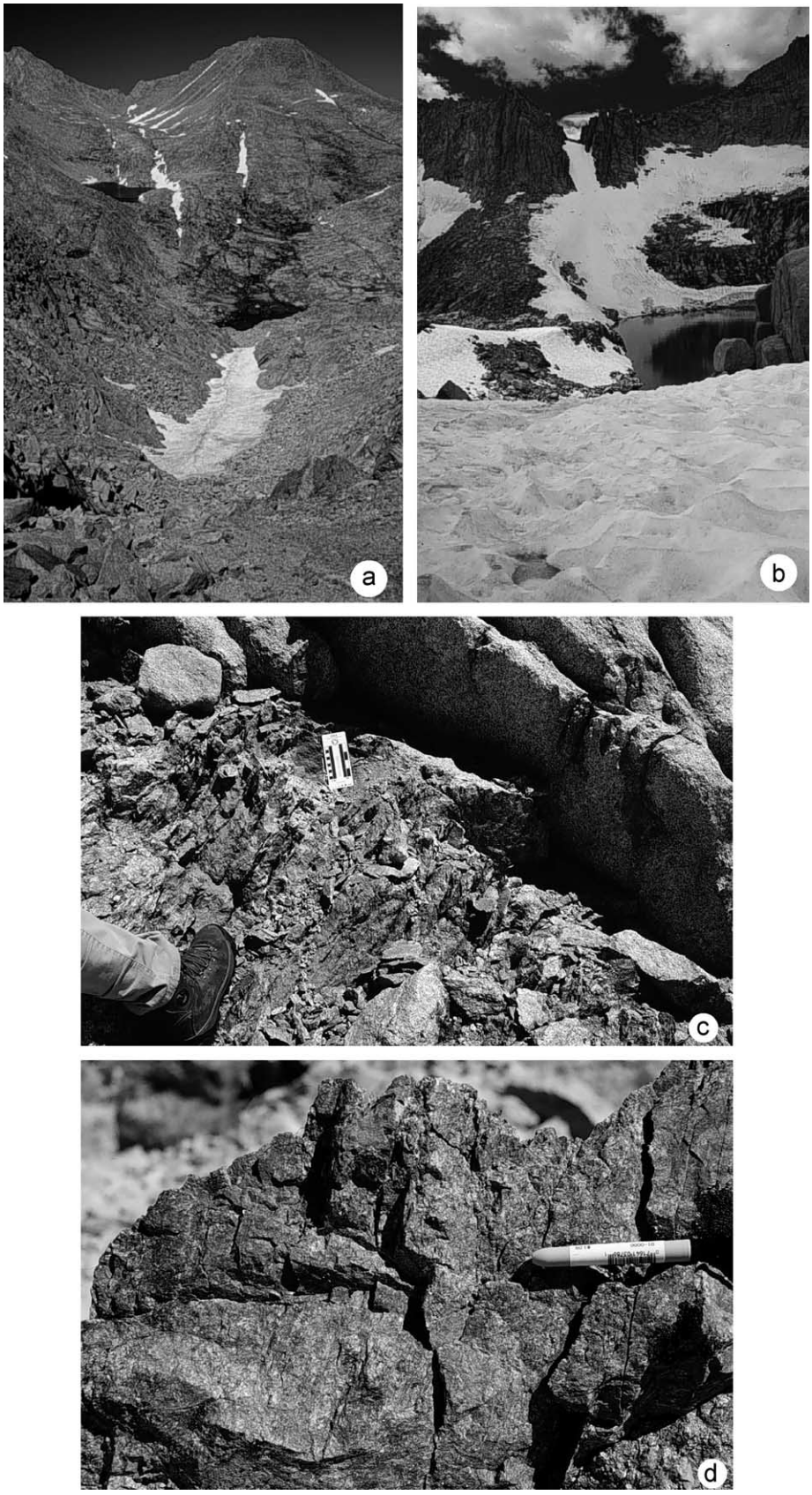
a
b
c
d

Table 1
Summary of orientation and slip data for the three segments of the Gemini fault zone

Segment	Orientation[a] (strike,dip)	Slip vectors[b] (trend, plunge)	S_{max}	Tip structures and notes on the structure of the segment
Three-Island Lake	032, 61° SE	179°, 20°	131 m	Curved horse-tail splay structures at western tip
	044°, 80° SE	200°, 21°		
	078°, 80°SE	259°, 11°		
Gemini Lake	060°, 60°N	245°–275°, 5–15°	57 m	Straight fault trace at west; possibly has Seven Gables fault terminating against it
Royce Lakes	050°, 80° NW	230°, 0–5°		
	040°, 83°NW	220°, 0–5°		
	025°, 85° W	205°, 10–20°	48 m	Segments 50–950 m long with left steps; SW tip consists of fault strands, NE tip terminates into joint sets

[a] Orientations listed from the western to the eastern end of the fault segment.
[b] Slip vector orientations listed from the western to the eastern end of the segment.

segments, identified from the slip-distance profile that is discussed below, include, from west to east, the Three Island Lake segment, the Gemini Lake segment, and the Royce Lakes segment (Fig. 3). Details regarding fault orientation, slip vector orientation, maximum slip, and notes regarding the fault structure are summarized in Table 1.

5.1.1. The Three Island Lake segment

The eastern part of the Three Island Lake segment trace descends west from the summit of Gemini Peak (3915 m) in a 3–8-m-wide fault trough that changes to a steep ~50-m-high, north-facing fault trough wall (Fig. 6, area A). The fault strikes east-northeast to northeast, dips steeply, and has shallowly west-southwest-plunging slip vectors (Fig. 6; Table 1). Along the central part of the fault (Fig. 6, area B), another lineament joins the Gemini fault through a series of termination splays oriented ~30° counterclockwise to the connecting strand (Fig. 6, area B). Southwest of point B, the fault zone trace arcs to the southwest in a complex network of fractures to form a horse-tail termination structure and a right step (Fig. 6, area C). The horse-tail structure contains three 0.3–0.5-km-long splays that strike south and southeast. A right step joins the curving horse tail structure to a straight, northeast-striking, southeast-dipping fault that terminates near Three Island Lake (Fig. 6). Near the lake, slip along the fault tapers to zero. The right step contains nearly vertical fault planes with slickenlines that shallowly plunge to the west.

5.1.2. The Gemini Lake segment

The Gemini Lake segment is composed of a relatively straight, steep northwest-dipping fault surfaces with nearly horizontal slickenlines (Fig. 7; Table 1). An unusual feature of this segment is the bend in the fault zone map trace that occurs at the summit of a mountain informally called '12221 peak' (Fig. 7, area A). Here, the fault zone trace bends 37° to the north. Although some of this bend may be due to topographic effects of the mountain peak and the northwest dip of the fault surface, a similar bend is observed on aerial photos ~0.3 km to the north-northeast (Fig. 7, area B). Less than 500 m to the north of the Gemini Lake segment, a prominent lineation trends parallel to the Gemini fault zone and terminates into it by a series of left-stepping splays, which are ~30° CCW relative to the main strand (Fig. 7, area C). We infer that this lineament is a left-lateral strike-slip fault zone and informally call this strand the Seven Gables fault zone (SGFZ). Near Gemini Lake, the splays of the SGFZ termination dip steeply and strike north-northeast (Fig. 7). This zone consists of highly fractured, dark brown–green rocks of the Lake Edison granodiorite that are heavily coated with chlorite, epidote, and iron oxides. The main trace of the Gemini fault zone in this area is marked by a snow-filled trough and a perennially

Fig. 5. Field photographs of the Gemini fault zone. (a) Photograph of the snow-filled topographic depression (left of the prominent peak) that defines the Gemini fault zone. View is to the northeast from the shoulder of 12221′ Peak. (b) Photograph of the snow-filled Gemini fault trough (linear snow patch in background) crossing through Royce Lakes in the foreground. View is to the west. (c) Photograph of highly brecciated fault core (around geologist's foot) separated from undeformed protolith (upper right) by bounding fault (above scale card). Scale card is 16.5 cm in length. (d) Close up photograph of chlorite breccias within the Gemini fault core. Length of pen is 13.5 cm. Views of (c) and (d) are to the south along the Royce Lakes segment of the Gemini fault zone.

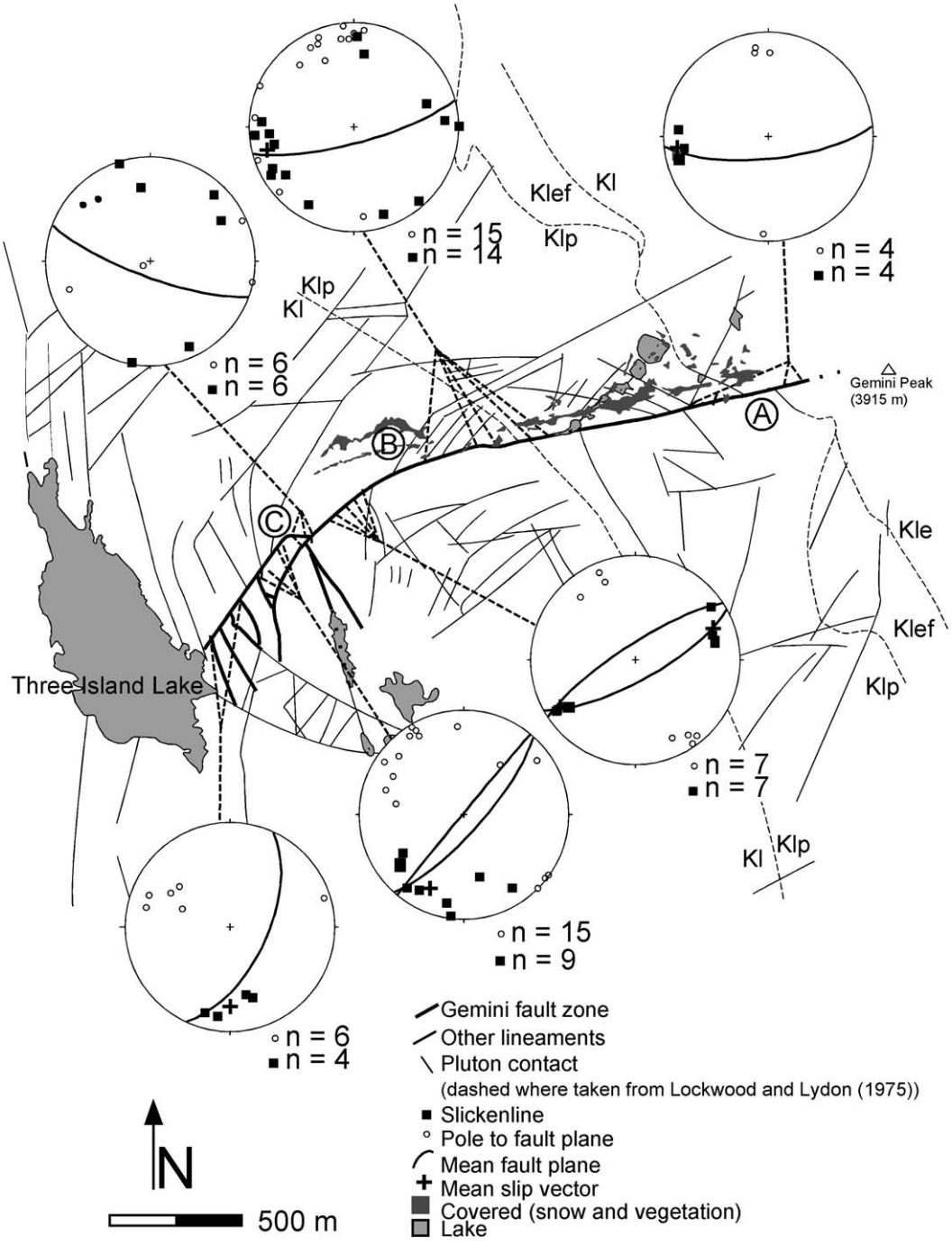

Fig. 6. Map view of the western segment of the Gemini fault zone, the Three Island Lake segment. Stereonets are lower hemisphere, equal area projections of poles to fault planes, slickenlines, mean fault plane (great circle), and mean slickenline (diamond). Upper left stereonet does not have mean slip vector because the data is too scattered to give meaningful results. Kl = Lamark granodiorite; Klp = porphyritic Lamark granodiorite; Klef = fine-grained facies of the Lake Edison granodiorite; Kle = Lake Edison granodiorite (Lockwood and Lydon, 1975).

frozen lake, informally termed 'Gemini Lake'. The fault zone left-laterally displaces the western contact of the Kqm1 body by ~40 m.

5.1.3. The Royce Lakes segment

The Royce Lakes segment is the easternmost segment of the Gemini fault zone and is composed of numerous fault strands that range from 50 to 950 m in trace length. The fault planes within this segment strike dominantly southwest, are vertical or dip steeply northwest, and slickenlines are nearly horizontal or plunge slightly west (Fig. 8; Table 1). At the ends of some fault strands, left steps connect to adjacent strands via 50–300-m-long splays oriented 35–65° counterclockwise (CCW) from the main strands (Fig. 8, point A).

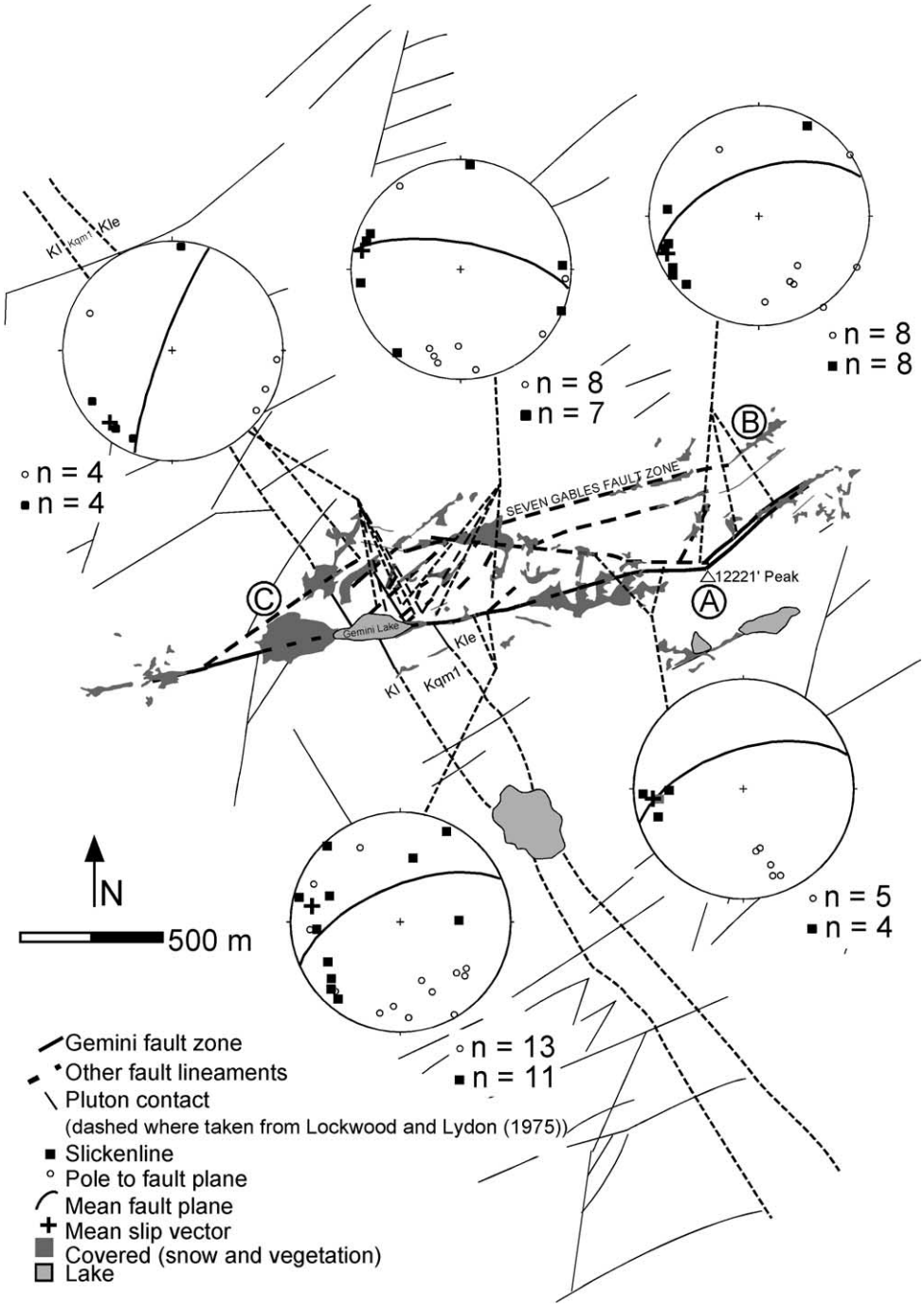

Fig. 7. Map view of the central segment of the Gemini fault zone, the Gemini Lake segment. Stereonets are lower hemisphere, equal area projections of poles to fault planes, slickenlines, mean fault plane (great circle), and mean slickenline (diamond). Kl = Lamark granodiorite; Kle = Lake Edison granodiorite; Kqm1 = quartz monzonite/granite (Lockwood and Lydon, 1975).

The southwest part of the segment is characterized by a complex network of subparallel fault strands, whereas the northeast part of the segment is a less complex system of parallel strands that are widely spaced and less connected by splay fractures. East of Royce Lakes, the fault terminates into a snow-filled trough that parallels the regional northeast–southwest-striking joint set (Fig. 8, point B). Here, the slip across the fault zone diminishes to $\leq$1 m, the amount of mineralization decreases, and slickenlines are scarce.

5.2. Slip-distance analysis

The degree of fault interaction is important for understanding fault growth and linkage (Peacock and Sanderson, 1991, 1994; Dawers and Anders, 1995; Gupta and Scholz,

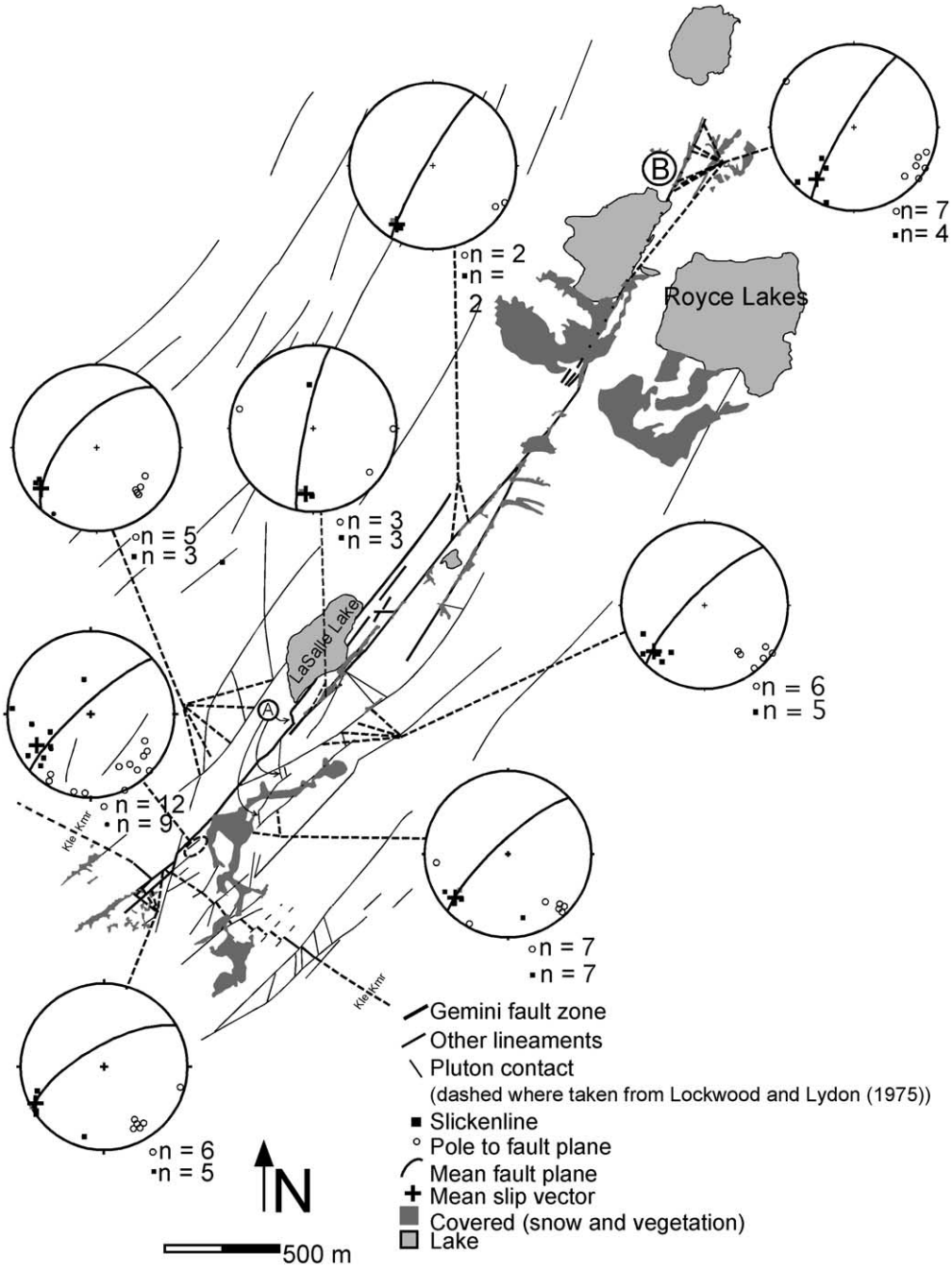

Fig. 8. Map view of the eastern segment of the Gemini fault zone, the Royce Lakes segment. Stereonets are lower hemisphere, equal area projections of poles to fault planes, slickenlines, mean fault plane (great circle), and mean slickenline (diamond). Kle = Lake Edison granodiorite; Kqm1 = quartz monzonite/granite (Lockwood and Lydon, 1975).

2000). There are two ways of estimating fault interaction: separation-overlap ratios and displacement-length (D-L) profiles. Separation-overlap ratios, the ratio of the distance between adjacent faults to the amount of adjacent fault overlap, does not reveal much about the state of interaction within the overlap zone (Gupta and Scholz, 2000). Displacement-length profiles are typically shown for normal faults of varying length and displacement. The focus here is on slip-distance analysis (S-D), rather than displacement-length analysis, which compares faults of differing length.

Slip-distance profiles are rare for strike-slip faults because few markers intersect faults at high angles to provide enough data on net slip (Gillespie et al., 1992). The slip-distance profile for the Gemini fault zone that is constrained by 16 offset markers that include steeply dipping aplite dikes, pluton contacts, and schlieren bands. Slip is calculated by determining the true dip of the marker

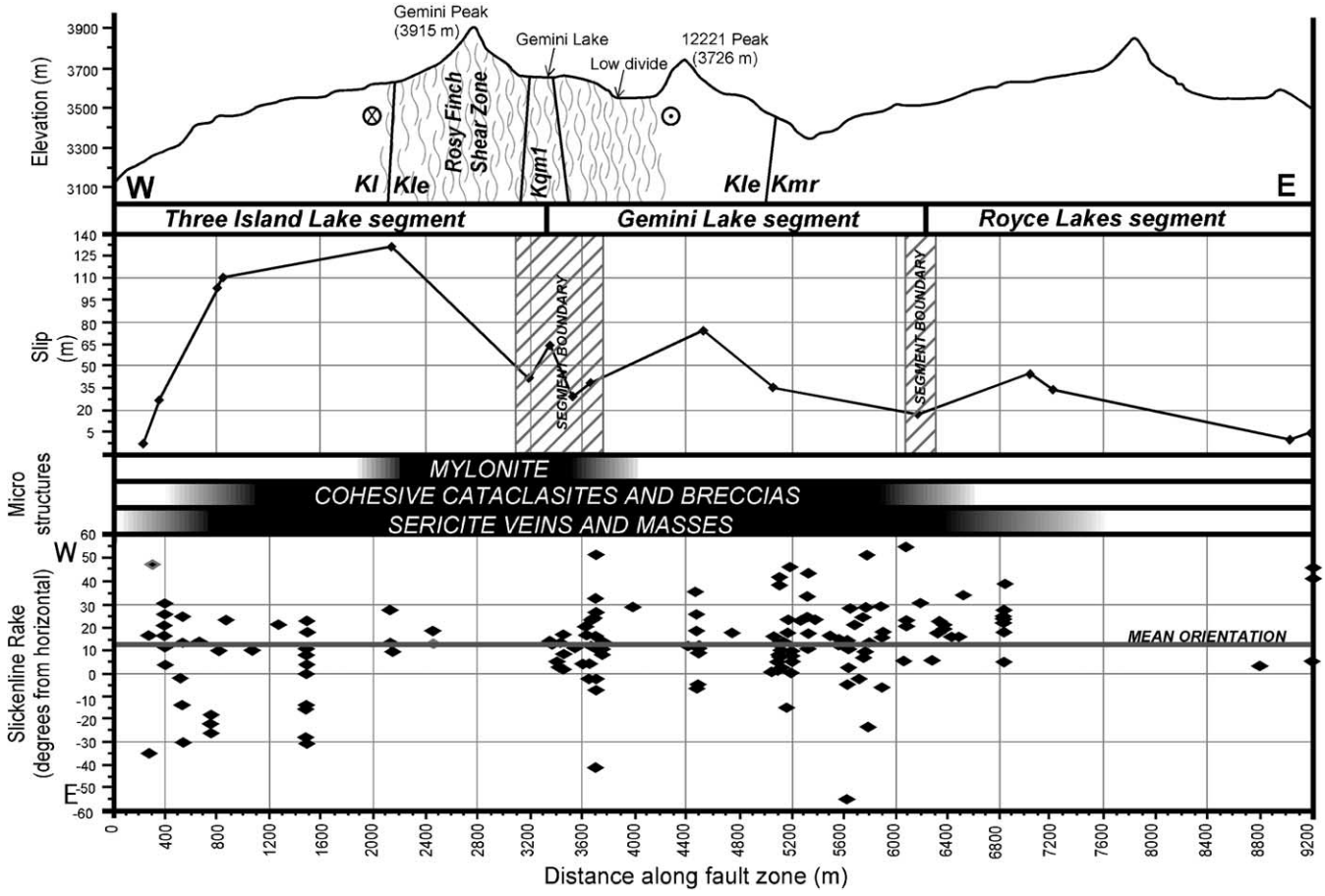

Fig. 9. East–west cross-section of the Gemini fault zone. Section shows topography (V.E. = 1.6), lithologies, the Rosy Finch shear zone (after Tikoff and Saint Blanquat, 1997), displacement-distance profile with segment boundaries, microstructural distribution, and slickenline orientation. White areas within the microstructures section represent regions that contain slipped epidote-coated joints.

feature on the fault plane and then creating a scaled-map view and cross-sectional diagram of the fault, the offset markers, and the local topography. Net slip was then measured from the scaled cross-sectional diagram.

The S-D profile for the Gemini fault zone is irregularly shaped, has four local maxima, and has a maximum slip of 131 m in the western third of the fault zone (Fig. 9). This creates a jagged, asymmetric profile skewed to the west. The S-D plot shows two regions of local slip minima. These slip minima were used to define the three segments of the fault zone, the Three Island Lake segment, the Gemini Lake segment, and the Royce Lakes segment, with respective surface trace lengths of 3.2, 2.8, and 3.0 km (Fig. 9).

The maximum slip occurs on the southwestern third of the fault zone (Three Island Lake segment). Local slip maxima are near the midpoint of the Gemini Lake segment and northeast third of the fault zone (Royce Lakes segment). Although the three segments are nearly equal in length, the maximum slip for the Three Island Lake segment is 131 m, nearly 2–3 times that for the Gemini Lake and Royce Lakes segments (Fig. 9). Interestingly, the local slip maximum is greatest on the segment that cuts the oldest pluton and least in the segment that is entirely in the youngest pluton, suggesting that faulting might have first begun in the oldest pluton. The slip gradient is also steepest at the western end of the Three Island segment, where slip decreases from 110 to 0 m over a distance of 800 m.

5.3. Joint data

We recorded attitudes for joint and fault planes in the Lamark, Lake Edison, and Mono Creek plutons to see whether the Gemini fault zone is composed of faults that share similar orientations to the joints (Fig. 10). In most cases, the orientations of the joints and the faults coincide. In the Mono Creek pluton the joints display two dominant strikes of ~135° and ~225°. The faults have one dominant strike of ~225° and both joints and faults dip steeply northwest and southeast. In the Lake Edison pluton, the joints and faults have one dominant strike of ~243° and dip steeply northwest (Fig. 10). The orientations of the joints in the Lamark pluton show more variability when compared with the Mono Creek and Lake Edison plutons (Fig. 10). There are three dominant joint strikes of ~252°, ~285°, and ~315° that dip northwest, north, and northeast, respectively. Faults in the Lamark pluton have two dominant strikes of

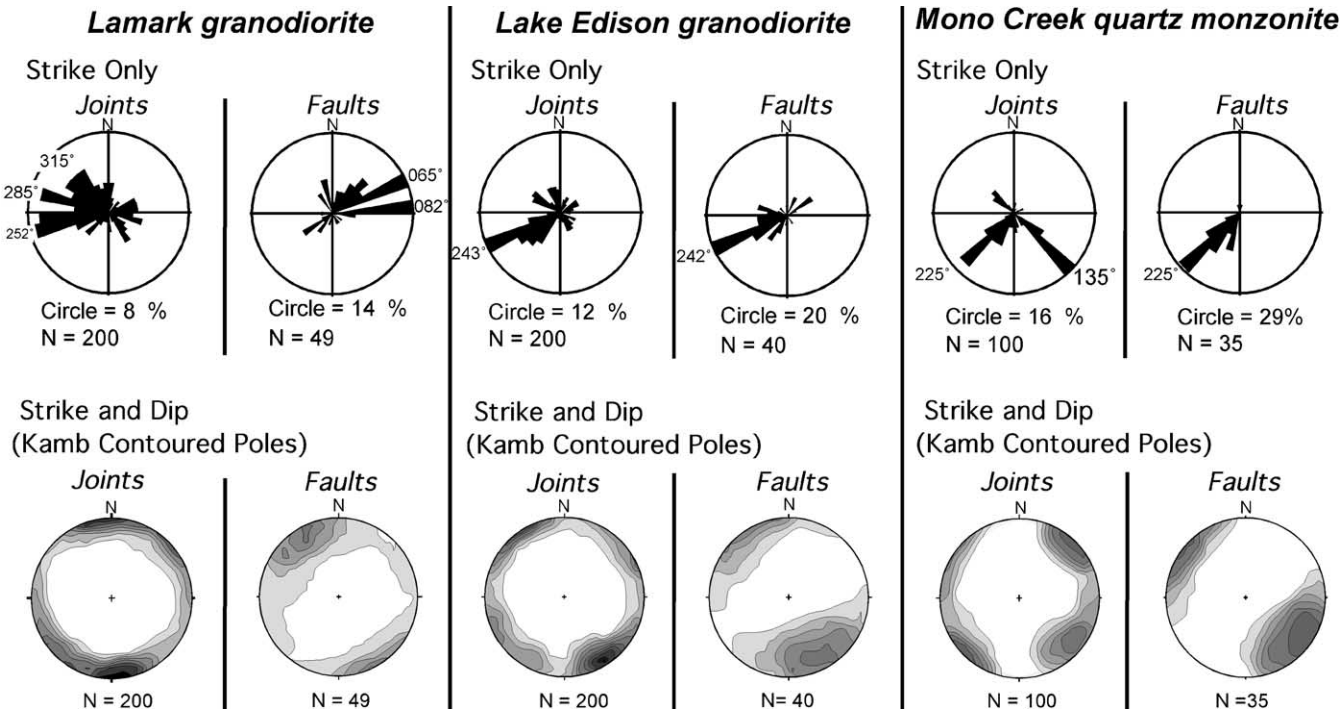

Fig. 10. Joint and fault comparison. Rose diagrams of joint and fault plane strikes and lower hemisphere equal area stereoplots of Kamb contoured poles to joints and faults in the Lamark granodiorite (left), Lake Edison granodiorite (center), and the Mono Creek quartz monzonite (right). The data show that the faults have similar orientations, in map view and in three dimensions, as the joints.

~065° and ~082° and dip steeply southeast and east-southeast.

When comparing the Lake Edison and Mono Creek plutons, the former has a greater number of joint sets (Fig. 10). The increased density and number of joints sets could reflect the ages and thermal histories of the plutons (S.J. Martel, 1999, pers. commun.). The Mono Creek pluton, which is the youngest of the three plutons, has been subjected to thermal stresses involved in its own emplacement and cooling. The older Lake Edison pluton might have had joint sets from its cooling as well as the heating/cooling cycle associated with the emplacement of the Mono Creek pluton. The Lamark pluton, the oldest of the three, may have been subjected to thermal stresses from its emplacement as well as emplacement of the Lake Edison and the Mono Creek plutons, and is thus likely to have higher joint densities and more diverse joint orientations.

5.4. Slickenline distribution and orientation

Variations in slip vector orientations over an entire fault zone are traditionally thought to reflect long-term changes of fault behavior or multiple tectonic events (Roberts, 1996; Shipton and Cowie, 2001). Recently, however, some workers show that during earthquakes fault zones may exhibit slip vector (rake) changes along strike and at a single location (e.g. Guatteri and Spudich, 1998). For example, the Nojima and Rokko fault systems during the 1995 Kobe earthquake (Bouchon et al., 1998; Spudich et al., 1998) and the San Andreas fault during the 1989 Loma Prieta earthquake (Beroza, 1991) produced curved and cross-cutting slickenlines where the fault surface was exposed.

Guatteri and Spudich (1998) provide a mechanical explanation for these observations through 3D boundary modeling of temporal slickenline orientation variability during earthquake rupture propagation. They conclude that rake variability is characteristic of fault zones that meet two criteria: (1) a low initial shear stress (~10 MPa) on the fault surface (i.e. the shear traction before an earthquake initiates), and (2) spatial variations in the direction of initial stress. Guatteri and Spudich (1998) conclude that, for low stress events, fault zone geometry is the dominant control of rake variability observed along fault surfaces.

Slickenlines of the Gemini fault zone are measured as the acute angle from horizontal and are broken into two broad categories: rakes that fall in the eastern and western stereonet hemispheres. Most slickenlines on the fault plunge to the west and, at any given site, there is significant variability. For example, data from several sites show >40° of rake variability and data from the station located ~5.6 km along the fault zone show ~85° of rake variability (Fig. 9). Data points stacked vertically on top of each other indicate more than one orientation at a station. The data show that: (1) 74% of the slickenline data are oriented between horizontal and 30° down from the west; (2) most of the fault is dominated by strike-slip movement; the mean and median orientations are 12° and 16° west

Fig. 11. Photograph of mylonite described in text. The foliation is left-laterally deflected in the shear zone. Photograph is taken near Gemini Lake. Length of pen is 15 cm.

with a standard deviation of 19° west, respectively; and (3) there is significant variability in slickenline orientation across segment boundaries.

5.5. Microstructures

In this section we present data on microstructures of the fault-related rocks in order to characterize the textures and deformation mechanisms of the fault zone. Unlike the plutons, the fault zone contains significant amounts of chlorite, epidote, quartz, sericite, and muscovite. These observations are supported by Segall and Pollard (1983a,b) and Robeson (1998) who, working on smaller fault zones ~2 km to the north, noted all of the above minerals and calcite and zeolites. The mineralogy and the microstructures suggest that the fault zone rocks were deformed at lower greenschist facies conditions. Qualitative descriptions of microstructures and mineral assemblages of 51 thin sections show that three distinct groups of structures/assemblages exist: mylonites, cohesive cataclasites and breccias, and sericite veins and masses.

5.5.1. Mylonites

Mylonite crops out along the center of the fault zone over a lateral distance of ~1.5 km or 16% of the surface trace length (Fig. 9). The mylonites extend from the west slope of Gemini Peak at an elevation of ~3915 m to the low divide east of Gemini Lake at an elevation of ~3634 m (Fig. 9). The mylonites are zones ~1–3 m long, often terminate into a brittle fracture over the distance of 1–2 m (Fig. 11), and appear to be obliterated by the larger brittle faults that comprise the fault core. We use the term brittle fault here to describe epidote and chlorite coated planar fractures that preserve slickenlines. In thin section, the mylonite consists of kink bands of biotite, quartz subgrains, mosaics of fine-grained, serrate-grain boundary quartz, and mica and quartz subgrain tails on mantled feldspar and quartz grains (Fig. 12a and b). Rotated delta- and phi- type feldspar porphyroclasts, *S–C* fabrics, and mica fish indicate left-lateral sense of shear (Fig. 12a and b). In some sections, the grain size of dynamically recrystallized quartz grains is significantly reduced from ~2 to ≤0.15 mm (Fig. 12b), indicating prolonged periods of strain at elevated temperatures. The imbricated clasts and bands of mica and dynamically recrystallized quartz define a vertical, east-northeast-striking foliation that roughly parallels the strike of the Gemini fault zone in this area.

5.5.2. Cohesive cataclasites and breccias

The oldest suite of structures to cut the ductile structures are fault-parallel bands of cohesive cataclasites and breccias. Following Passchier and Trouw (1996), we use the term cohesive cataclasites for rocks having <30% by volume of angular fragments of the wall rock or fractured veins in a fine-grained matrix and cohesive breccias have >30% by volume of fragments in a fine-grained matrix. The cohesive cataclasites and breccias were observed in samples collected over a lateral distance of 6.8 km or 73% of the fault zone's trace length (Fig. 9). They appear to be concentrated in the western half of the fault zone, and become increasingly clast-supported where the texture dies out. The cataclasite and breccia bands range in thickness from ≤1 to >50 mm (entire thin-section width) and reach lengths >76 mm (entire thin-section length). In outcrop, some bands are several centimeters thick and extend along the fault for several meters. These textures contain angular clasts of feldspar and dynamically recrystallized quartz that range in size from ≤0.1 to >35 mm and are surrounded by an optically unidentifiable matrix of very fine-grained, dark material that is likely to be oxides and very fine-grained chlorite (Fig. 12c). The cataclasite and breccia bands are cut by sericite veins and areas of sericitization, demonstrating that the formation of the dark cataclasites and breccias predates the sericitized textures described next.

5.5.3. Narrow sericite-filled veins

Transgranular sericite-filled veins are observed nearly the entire length of the fault zone (Fig. 9). It is likely that these structures extend farther east to the end of the fault, but limited exposure and steep cirque head walls prevented sampling in those areas. The western termination of the texture approximately corresponds to the end of the fault zone. They occur in a variety of orientations relative to the

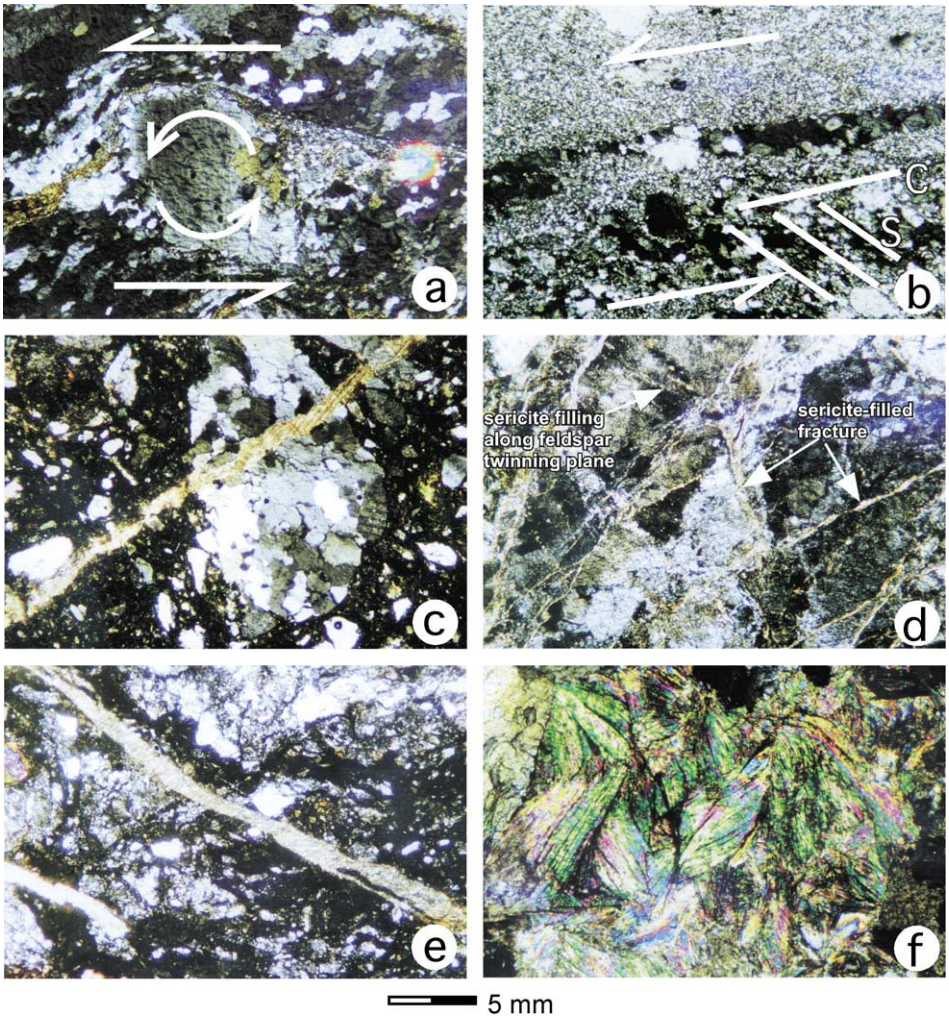

Fig. 12. Photomicrographs of the Gemini fault zone microstructures and mineralization. All views are with cross polarized light. (a) Rotated s-type core-mantle porphyroclast showing left-lateral sense of shear. View is oriented parallel to the fault strike. (b) Bands of dynamically recrystallized quartz and feldspar showing a weakly developed *S–C* fabric. View is oriented perpendicular to the fault plane and parallel to the slip vector. (c) Cohesive breccia with a dark oxide matrix and clasts of dynamically recrystallized quartz. Sericite-filled vein cuts fine grained-matrix and clasts, indicating late-stage vein filling. View is oriented perpendicular to the fault plane and perpendicular to the slip vector. (d) Brittle fracturing and sericite vein filling. Some veins form along preexisting weaknesses in the material, such as feldspar twining planes, *S–C* foliation planes, and grain boundaries, whereas others seem to cut across grains without preference. The veins range in thickness from ~0.1 to 1.0 mm. View is oriented perpendicular to the fault plane and parallel to the slip vector. (e) Well developed sericite fibers. Vein cuts fine-grained matrix and clasts, indicating growth into an open fracture under static conditions. View is oriented perpendicular to the fault plane and parallel to the slip vector. (f) Well developed sericite crystals. The large size of these crystals suggests that there was a prolonged period of static recrystalization. View is oriented perpendicular to the fault plane and perpendicular to the slip vector.

dominant fault surface. Some veins appear to open along preexisting weaknesses in the material, such as feldspar twining planes, *S–C* foliation planes, and grain boundaries, while others seem to cut across grains (Fig. 12d). The veins range in thickness from ~0.1 to ~3 mm. Continuous fibers span many vein openings, indicating that the sericite has grown in an opening mode fracture during static recrystalization (Fig. 12e). We observe only one generation of sericite veins in the thin sections.

5.5.4. Wide masses of sericite

The youngest textures, which formed in conjunction with the narrow sericite veins, are masses of sericite crystals. Some masses cover entire thin sections and others occur in distinct veins. The mineralization occurs as a complex patchwork of interlocking grains (Fig. 12f). Our thin-section observations suggest that this texture grew, or was sourced from, the narrow sericite veins discussed above and may represent an advanced stage of mineralization. The grains do not show any evidence of deformation, such as bent or folded folia, suggesting that the grains grew via static recrystalization into multigranular voids.

5.5.5. Cross-cutting relationships

Cross-cutting relationships suggest that the microstructures evolved from early ductile to later brittle structures. The mylonites described above are the oldest microstructures observed along the fault zone. They are cut by the

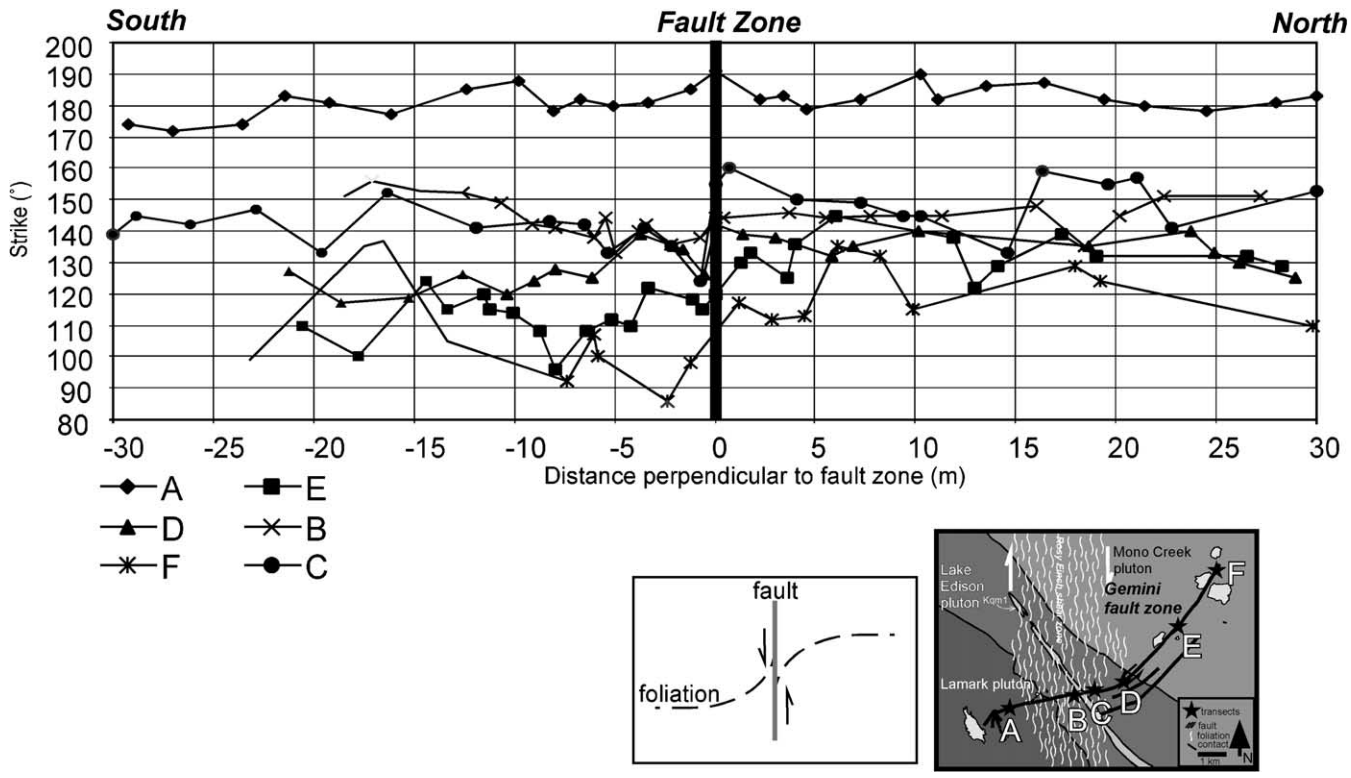

Fig. 13. Strike of foliation versus distance from fault zone. Magmatic foliation was measured at six locations (starred on inset location map) along the Gemini fault zone to determine if the Gemini fault zone deformation was distributed across an area wider than the fault trough. If this were the case, the magmatic foliation should be deflected into the fault zone (see inset figure). The lack of any apparent deflection indicates that the deformation along the fault zone was concentrated in the fault trough under brittle conditions.

cohesive cataclasites and breccias. The cohesive cataclasites and breccias contain angular clasts of dynamically recrystallized quartz and feldspar (Fig. 12c). There are no discernable cross-cutting relationships between the cohesive cataclasites and the cohesive breccias. The mylonites and the cohesive cataclasites and breccias are cut by the narrow sericite-filled veins and the wide masses of sericite (Fig. 12d–f), suggesting that the dominant period of mineralization occurred after deformation. The mineralization via the narrow sericite veins and the wide masses of sericite appear to overprint all other microstructures and is observed the entire length of the fault zone.

5.6. Magmatic foliation transects

Microstructures from the Gemini fault zone indicate that, for most of the fault zone's trace length, slip is concentrated on narrow (<5 cm wide) bands within a 2–15-m-wide fault trough dominated by brittle deformation processes. To assess how deformation along the fault zone has been accommodated, we measured attitudes of magmatic foliation in six 30-m transects oriented perpendicular to the fault trough (Fig. 13). Areas along strike of the fault zone that experienced distributed strain should exhibit rotation of the magmatic foliation towards the center of the fault zone, reflecting the fault zone's sense of shear (i.e. deflected foliation into a shear zone; see inset Fig. 13). The data for the foliation surrounding the Gemini fault zone show no apparent rotation or drag into the fault zone. This implies that the fault zone has always been deformed in the brittle regime and that all left-lateral strike-slip deformation is confined to the fault trough. The attitude of the foliations measured in the 30-m-long transects are consistent with those recorded by Lockwood and Lydon (1975) farther away from the fault zone. This indicates that, when examined at the map-scale, all deformation associated with the fault zone is confined to the narrow fault trough.

6. Discussion

This paper presents field-based structural analyses of the geometry, kinematics, slip-distribution, and microstructures of a ~10-km-long, left-lateral strike-slip fault zone. We evaluate five aspects of the data presented here: (1) fault-zone scaling; (2) controls on the geometry of the fault zone; (3) the slip-distance profile; (4) slickenline orientation; and (5) lateral composition of the fault zone.

6.1. Fault scaling

The Gemini fault zone consists of three segments composed of a highly brecciated and mineralized fault

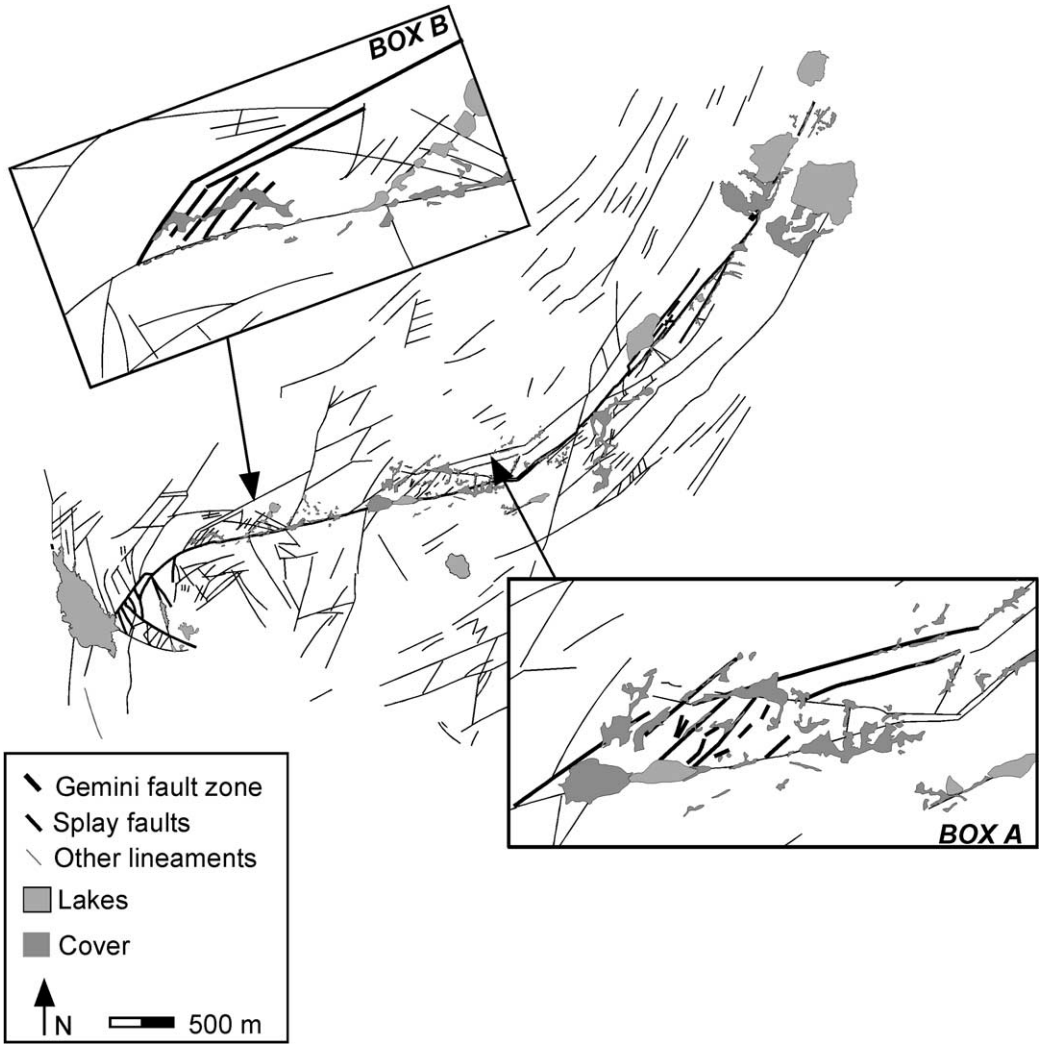

Fig. 14. Examples of splay faults that link adjacent fault zones to the Gemini fault zone. These structures resemble analogous meter-scale structures documented by Martel et al. (1988) and Martel (1990).

core that is in sharp contact with undeformed protolith. The core, ~2–15 m wide, is bounded by mineral coated, polished, and striated fault surfaces. Little to no damage zone is observed. Many of the aspects of fault zone structure we observe here are similar to the relationships documented by Martel et al. (1988), and Martel (1990) suggests that the architecture of the left-lateral strike-slip faults in this area may be scale invariant over scales of 10 m to 10 + km.

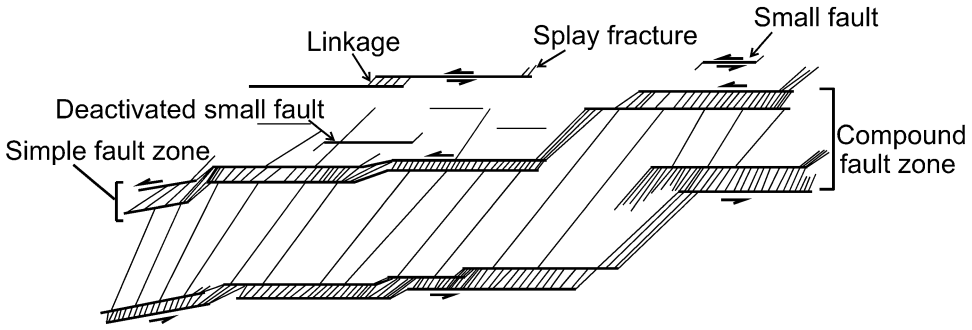

Fig. 15. Progression of meso-scale fault development (modified from Martel, 1990, fig. 2d). Small faults develop into simple fault zones, which become compound fault zones with increasing slip. Structures, such as fault linkages and terminations, are observed at the map-scale in the Gemini area; however, the width of the compound fault zone and linkage fractures do not scale proportionately.

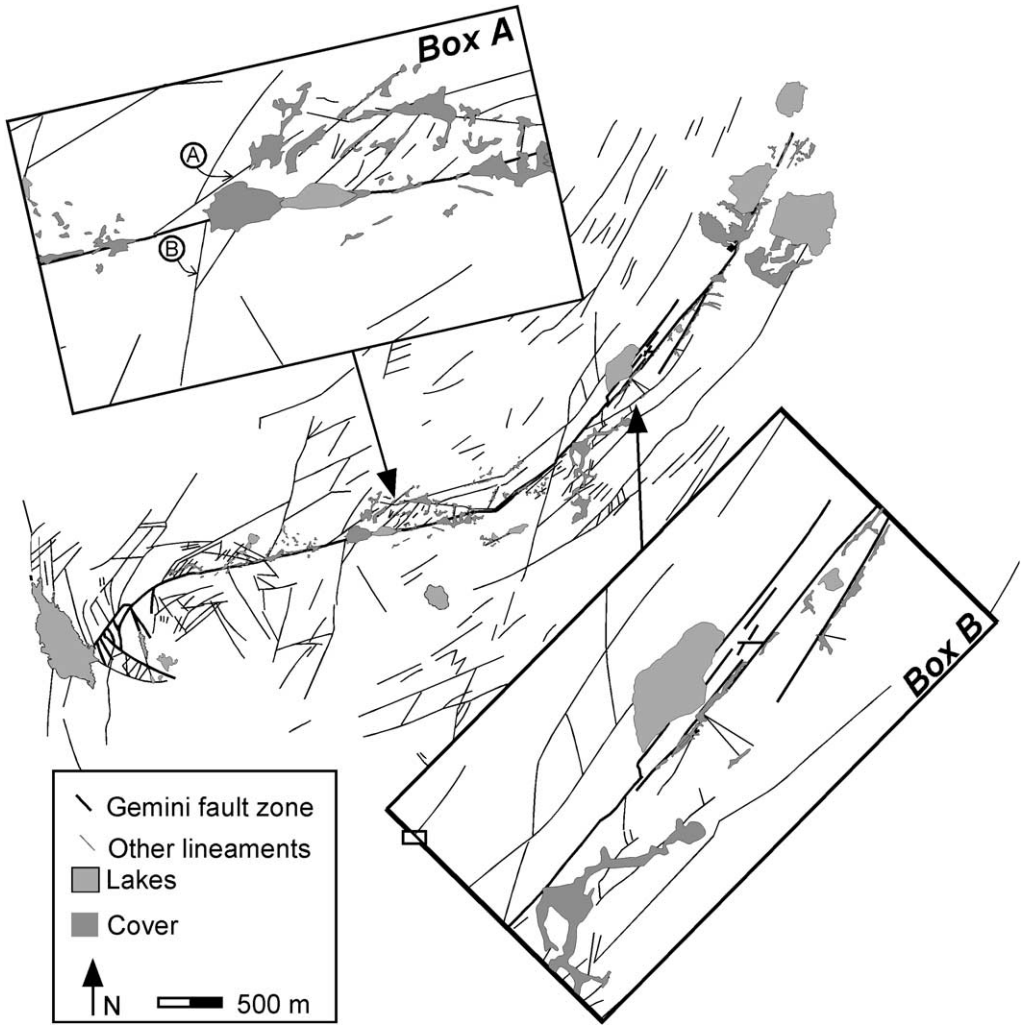

Fig. 16. Close up of segment boundary zones. The occurrence of Three Island Lake/Gemini Lake segment boundary (box A) may be the result of: (1) the Seven Gables fault zone terminating into the Gemini fault zone, creating an apparent slip deficit near Gemini Lake (box A, point A), or (2) the NNE–SSW striking fault that intersects the Gemini fault zone from the south (box A, point B). We hypothesize that slip may have been transferred to this subsidiary fault zone, resulting in the displacement minima at this locale. The Gemini/Royce Lakes segment boundary may be the result of the increased density of subsidiary faults in this area. The area coincides with a subtle change in joint orientations from NE–SW (box B, point A) to NNE–SSW (box B, point B). It is likely that the slip deficit recorded along the Gemini fault zone in this area is the result of the subsidiary faults accommodating some slip.

Examples of fault linkage can be seen at two locations along the Gemini fault zone (Fig. 14). The left-stepping termination of the Seven Gables fault zone (SGFZ) into the Gemini fault zone (Fig. 14, box A) is an example of a kilometer-scale analog of the meter-scale linkage described by Martel (1990) (Fig. 15). The geometry and kinematics of this linkage zone are consistent with the meter-scale simple and compound fault zone models of Martel et al. (1988) and Martel (1990). Another example of this type of structure is observed on the Three Island Lake segment. Here, a series of left-stepping lineaments connect two northeast-striking lineaments to the southwest-curving Gemini fault zone (Fig. 14, box B). The left-stepping lineaments are oriented ~30° CCW from the northeast-striking lineaments and appear to terminate at the Gemini fault zone.

Martel (1990) classifies the Gemini fault zone as a 'compound fault zone', a complex fault system that is composed of 'simple fault zones' (Martel et al., 1988) (Fig. 15). Although the outcrop-scale structure of the Gemini fault zone seems to scale from the 'simple faults zones' of Martel et al. (1988) (see Martel (1990) for details), when examined at the 10-km scale there are aspects that clearly do not scale from the smaller faults.

1. The *general* geometry of the fault zones are different. The ~10-km-long Gemini fault zone has a curved map pattern while most of the fault zones of Martel et al. (1988) and Martel (1990) have, for the most part, relatively straight map traces.
2. Martel (1990) shows that simple fault zones link via splay fractures to form compound fault zones (Fig. 15). The ratio of the simple fault-zone width to the length of the splay fractures is ~1:9 (Fig. 15). If adjacent compound fault zones link in a similar manner and if

they scale proportionally, one would expect the ratio of fault-zone width to splay length to be similar. Examining the two areas where kilometer-scale splay fractures link the Gemini fault zone to adjacent fault zones (Fig. 14, boxes A and B), a conservative estimate of the ratios of fault-zone thickness to splay-fracture length are much higher, ~1:25. In these two areas, the fault zone is ~20 m wide and the splay fractures that link the adjacent fault zone to the Gemini are, on average, ~500 m long. This indicates that, when examined at the 10-km-scale, geometries produced through fault zone linkage may not scale proportionally with the meter-scale, left-lateral strike-slip fault zones.

3. Our data show that the western termination of the fault zone resembles the structure described in Grannier (1985) and McGrath and Davidson (1995) rather than the splay-fracture terminations described by Martel et al. (1988), Martel (1990), and Segall and Pollard (1983b). The main structure mapped at the western end of the fault zone makes a broad arc to the southwest. Emanating from the main fault strand are a series of southeast-striking splays. The nature of the southwestern tip of the main fault trace suggests that the fault encountered an increased resistance to propagation caused by the lack of favorably oriented linkage structures as described for modeled faults by Martel (1999).

6.2. Controls of fault zone geometry

The size of the process zone, the areas of enhanced deformation at fault tips, are thought to scale with slip (Cowie and Scholz, 1992). As faults grow, inactivated process zones should be evident in the rock mass surrounding the fault. We do not observe a systematic increase in fracturing from the center of the fault trace towards its ends that might reflect the migration of a process zone and conclude that the fault did not propagate as a planar shear fracture in undeformed rocks. The fault seems to have grown instead by slip along the preexisting fractures and by their linkage (e.g. Segall and Pollard, 1983b).

The western termination of the Gemini fault zone is a curving horsetail structure. Here, the Lamark pluton has multiple joint sets of varying orientation and thus, the processes of fault-zone termination were different from those acting at the eastern end. Elastic modeling by Martel (1999) indicates that curving fault ends may develop if the resistance to slip increases significantly near the end of the fault. We hypothesize that the western termination of the Gemini fault zone may be a manifestation of these theoretical solutions. Examining the Gemini fault zone S-D data, the western third of the fault zone has accumulated most of the slip and has a steep (0.18) slip gradient on its western end (Fig. 9). Aerial photo analysis and field measurements (Figs. 6 and 10) indicate that the Lamark pluton, found at the fault zone's western end, may have multiple joint sets. As discussed above, this may have been the result of the complex thermal history of the pluton. The lack of suitable linkage structures or parallel joints sets may have caused an increased resistance to slip that could have resulted in the curved nature of the western termination of the Gemini fault zone.

6.3. Slip-distance analysis

Two important points that arise from the slip profile (Fig. 9) include evidence for physical linkage ('hard linkage'; Walsh and Watterson, 1991) of the fault zone at the segment boundaries and insights into how the fault grew based on current fault growth models. Each point is discussed below.

6.3.1. Structures at segment boundaries

Two zones bound segments along the Gemini fault zone (Figs. 9 and 16). The western zone occurs at Gemini Lake where the Three Island Lake and Gemini Lake segments converge (Fig. 16, box A). No steps or jogs in the fault zone are discernable at this point and linkage of the fault zone to other fault zones via splays is not apparent. The slip deficit in this region may be explained by the intersection of the Seven Gables fault zone with the Gemini fault zone, which resulted in an area of apparent slip deficit or the interaction of the Gemini fault zone and the northeast–southwest-striking splay fault that intersects the Gemini in this area.

The SGFZ terminates into the Gemini fault zone near Gemini Lake in a series of left-stepping splays (Fig. 16, box A, near point A). It is possible that the slip from the SGFZ was transferred to the Gemini fault zone along the westernmost splay. The sharing of slip between the Gemini Lake segment and the SGFZ would cause an apparent deficit on the Gemini Lake segment (Fig. 9). As an alternative hypothesis, the slip deficit may be the result of the mechanical interaction between the Gemini fault zone and the north-northeast-striking fault that intersects the Gemini fault zone at a high angle from the south, west of Gemini Lake (Fig. 16, box A, point B). It is possible that some of the slip was transferred to this fault, resulting in a slip deficit in this area.

The eastern segment boundary (the Gemini Lake and Royce Lakes segment boundary) roughly corresponds to the subtle change in joint orientations that is observed ~500–700 m east of the Mono Creek and Lake Edison pluton contacts (Fig. 16, box B). A slip deficit occurs in the area where the two joint sets overlap. In this area, faults and joints have a wide range of orientations, some traces are curved, and others are at high angles to the main fault-zone trace. We hypothesize that the slip deficit observed along the Gemini in this area may be the result of slip being accommodated by these subsidiary structures. An alternative interpretation for these slip minima is that they reflect regions of along-strike compositional variations that

inhibited fault propagation, and thus produced regions of low slip.

6.3.2. Fault zone growth

The slip profile is characterized by three local maxima and a steep slip gradient of ~0.18 at the western end of the fault zone. This gradient falls within the ranges of other published slip data of 0.002 to 0.25 as compiled by Shipton and Cowie (2001). Steep slip gradients have been interpreted to indicate fault linkage (Peacock and Sanderson, 1991, 1994; Willemse et al., 1996; Gupta and Scholz, 2000) or regions of high yield stress at the fault tip (Martel, 1999). In these models, steep slip gradients occur on the two neighboring ends of adjacent segments. Our data show the highest gradients on the western end of the Three Island Lake segment where there is no other visible interacting fault zone. The asymmetric slip profile observed on the Gemini fault zone might reflect the lack of suitable linkage structures in the Lamark pluton.

Gupta and Scholz (2000), using slip data from small normal faults and an elastic boundary element model, show that the local slip minima at a point of linkage becomes less apparent as the linked fault zone matures from a 'soft-linked' to a 'hard-linked' fault. They show that as a fault zone reaches an advanced stage of interaction, the slip profile resembles that of a continuous fault surface (e.g. Cowie and Scholz, 1992). If the model of Gupta and Scholz (2000) is correct and applicable to strike-slip fault zones, the presence of three local slip maxima and the asymmetry of the cumulative slip profile suggests that the Gemini fault zone did not have complete slip transfer through its segment boundaries and did not act as one continuous fault, or that fault activity ceased soon after linkage.

This topic is important for understanding why some segment boundaries efficiently transfer slip of propagating earthquake ruptures and others arrest slip. Here, we have a segmented ~10-km long, left-lateral strike-slip fault that shows apparent segmentation at two locales along its trace. As discussed above, the western segment boundary may not necessarily be a true segment boundary, but might reflect the junction of two fault zones, the Gemini and Seven Gables fault zones, that have created an apparent slip deficit. The eastern segment boundary, however, may be a segment boundary that has formed from the interaction of two joint sets of differing strike. In this area, we see that the segment boundary zone is composed of numerous smaller fault zones that curve or are at high angles to the main fault-zone trace.

Highly fractured and chaotic segment boundaries have been inferred at depth along seismogenic fault zones. It is unclear how and why slip is transferred through these zones. Felzer and Beroza (1999), for example, describe segment boundaries for the Emerson fault and the Homestead Valley fault, components of the 1992 Landers earthquake, as areas of structural complexity characterized by off-fault aftershock focal mechanisms. The eastern segment boundary of the Gemini fault zone appears to be an exhumed analog to the complex structures described by Felzer and Beroza (1999). Such a structure could produce focal mechanisms that do not lie upon the main fault trace.

6.4. Slickenline orientation

Our slickenline distribution data are inconsistent with the single-fault slip vector model of Roberts (1996), which shows systematic slickenline changes at segment boundaries (i.e. slip should become progressively steeper away from the center of an elliptical fault). Our data do not fit this model and may be explained by some combination of the following four ways:

1. The variable slickenline orientations may reflect stress perturbation during rupture (dynamic stresses). If this were correct, this would suggest that the ruptures that occurred along the Gemini might have been similar to the low initial shear stress and nonuniform stress directions described by Guatteri and Spudich (1998) and discussed above.
2. The range of slickenline orientation may be due to compositional variations along the fault zone.
3. The data may reflect different slip orientations at different times during the fault zone's history.
4. Roberts' (1996) model does not apply to ~10-km-long strike-slip faults.

If the model of Guatteri and Spudich (1998) is correct, it is possible that the slickenline variability observed along the Gemini fault zone resulted from its complex geometry and resulting stress heterogeneities.

6.5. Lateral composition of the fault zone

The distribution of mylonitic textures broadly corresponds to the intersection of the Gemini fault zone and the Rosy Finch shear zone (Fig. 9). Other workers in the region (e.g. Martel et al., 1990) observe mylonitic fabrics in ductile structures that are associated with meter-scale brittle faults. They conclude that the occurrence of the ductile structures increases towards the Lake Edison pluton/Mono Creek pluton contact and the ductile fault zones formed shortly after the emplacement of the Mono Creek pluton when the rock was near the brittle/ductile transition. These ductile structures are essentially the same as those observed along the Gemini fault zone. In the Gemini area, we observed ductile structures as far east as the Lake Edison granodiorite/Mono Creek granite contact (this locale was not along the Gemini fault zone) and as far west as the Lamark granodiorite/Lake Edison granodiorite contact (Fig. 9). The occurrence of the ductile structures *along the Gemini fault zone* better corresponds to the intersection with the Rosy Finch shear zone rather than the Lake Edison granodiorite/Mono Creek granite contact; however, we cannot exclude the possibility of the latter.

We attribute the occurrence of the cohesive breccias and

cataclasites to largely reflect protolith mineralogies. The Lake Edison and Lamark plutons contain a higher density of mafic minerals than the Mono Creek pluton. The mafic nature of the host rock may account for the occurrence of the dark oxide–chlorite matrix in the cohesive cataclasites and breccias.

Recent work on fault zone microstructures suggests that discrete slip surfaces form early in the fault zone's development and those processes remain operative as the fault zone grows (Evans et al., 2000). These conclusions apply to faults in granite (Robeson, 1998), faults in sandstone (Shipton and Cowie, 2001), and faults in mixed lithologies (Chester and Logan, 1986; Chester et al., 1993; Chester and Chester, 1998; Schulz and Evans, 1998). The distribution of microstructural textures and inferred processes along the Gemini fault zone indicate the following:

1. The same deformation mechanisms were active on all segments regardless of their amount of slip. We observe cohesive breccias and cataclasites on segments with >100 m of slip (Three Island Lake segment) and on segments with as little as ~35 m (Royce Lakes segment).
2. Microstructures evolved with changing conditions. The transition from high temperature mylonites or cohesive cataclasites and breccias to brittle cracking and sericite veining may reflect increased strain rates (e.g. Martel et al., 1988) or lower temperatures. The well-developed grains of sericite crystals, the youngest microstructure, observed along ~80% of the fault zone suggest that small cracks along the fault zone experienced periods of opening in the brittle regime. These observations imply that the fault zone had transient patches of fault material, perhaps low velocity zones that became high velocity zones, whose physical properties changed through time as the area cooled.

The distribution of mylonitic rocks near the center of the entire fault zone might indicate that they first formed in this region during waning stages of upper greenschist conditions. Subsequent slip as the area cooled rapidly (Segall et al., 1990) would have resulted in the overprinting of cataclastic textures on the mylonitic zone. The lack of correlation between slip maximum and the presence of the early formed mylonitic rocks would point to the influence of compositional heterogenities along the fault zone as influencing the slip distribution.

7. Conclusions

We show that the Gemini left-lateral strike-slip fault zone is composed of numerous steeply dipping, northeast- and southwest-striking fault planes that have mineral lineations that plunge gently to the southwest. The geometry and slip profile of the exhumed fault zone and surrounding lineaments examined here suggest that the fault zone grew from smaller, 2.5–3-km-long fault segments. The segments became linked through highly fractured zones and left-stepping splays to form a ~10-km-long fault zone. Joints and the fault zone have similar orientations and indicate that the fault zone geometry is controlled by the occurrence of preexisting joint sets. The slip-distance data show that the steepest slip gradient occurs at the western third of the fault zone and slip tapers to zero near the fault zone's eastern and western terminations. Slickenline orientations vary nonsystematically over the entire fault zone and segment boundaries. We have identified four microstructures that include mylonites, cohesive cataclasites and breccias, and two forms of sericitization, and represent deformation through lower greenschist facies conditions on narrow, brecciated slip surfaces. The distribution of the deformation mechanisms on all segments of varying slip magnitudes implies that the same deformation processes were active at slip magnitudes greater than 35 m. The extensive nature of the sericitization suggests that the fault zone was hydraulically connected during mineralization.

Acknowledgements

This research was funded by a U.S. Department of Energy Office of Basic Energy Sciences Grant DE-FG03-95ER14526 to Evans and an AAPG grant to Pachell. Assistance in the field and discussions with K. Jill Hammond were invaluable to the completion of this project. Collaborations with Steven J. Martel have helped us understand the structures of the High Sierras and the mechanics of faulting. Discussions and reviews of previous versions of this paper by Zoe Shipton, Susanne Janecke, and Peter Kolesar helped us to refine out ideas, and journal reviewers David Gray and Chris Wibberley helped us improve the paper significantly.

References

Ague, J.J., Brimhall, G.H., 1988. Magmatic arc asymmetry and distribution of anomalous plutonic belts in the batholiths of California: effects of assimilation, crustal thickness, and depth of crystallization. Geological Society of America Bulletin 100, 912–927.

Bateman, P.C., 1992. Plutonism in the central part of the Sierra Nevada Batholith, California. U.S. Geological Survey Professional Paper 1483, 186.

Ben-Zion, Y., 1998. Properties of seismic fault zone waves and their utility for imaging low-velocity structures. Journal of Geophysical Research 103, 12567–12585.

Bergbauer, S., Martel, S.J., 1999. Formation of joints in cooling plutons. Journal of Structural Geology 21, 821–835.

Beroza, G.C., 1991. Near-source modeling of the Loma Prieta earthquake: evidence for heterogeneous slip and implications for earthquake hazard. Bulletin of the Seismological Society of America 81, 1603–1621.

Beroza, G.C., Spudich, P., 1988. Linearized inversion for fault rupture behavior: application to the 1984 Morgan Hill, California, earthquake. Journal of Geophysical Research 93, 6275–6296.

Bouchon, M., Sekiguchi, H., Irikura, K., Iwata, T., 1998. Some characteristics of the stress field of the 1995 Hyogo-ken Nanbu (Kobe) earthquake. Journal of Geophysical Research 103, 24271–24282.

Chester, F.M., Logan, J.M., 1986. Implications for mechanical properties of brittle faults from the observations of the Punchbowl fault, California: internal structure of fault zones. Pure and Applied Geophysics 124, 79–106.

Chester, F.M., Chester, J.S., 1998. Ultracataclasite structure and friction processes of the Punchbowl Fault, San Andreas System, California. Tectonophysics 295, 199–221.

Chester, F.M., Evans, J.P., Biegel, R., 1993. Internal structure and weakening mechanisms of the San Andreas fault. Journal of Geophysical Research 98, 771–786.

Chiarabba, C., Amato, A., 1994. From tomographic images to fault heterogeneities. Annalli di Geofisica 37, 1481–1494.

Cowie, P.A., Scholz, C.H., 1992. Physical explanation for the displacement-length relationship of faults using a post-yield fracture mechanics model. Journal of Structural Geology 14, 1133–1148.

Dawers, N., Anders, M.H., 1995. Displacement-length scaling and fault linkage. Journal of Structural Geology 17, 607–614.

Evans, J.P., Shipton, Z.K., Pachell, M.A., Lim, S.J., Robeson, K., 2000. The structure and composition of exhumed faults, and their implications for seismic processes. In: Bokelmann, G., Kovach, R.L. (Eds.). Proceedings of the 3rd Conference on Tectonic Problems of the San Andreas Fault System. Stanford University, Stanford, pp. 67–81.

Evernden, J.F., Kistler, R.W., 1970. Chronology of emplacement of Mesozoic batholithic complexes in California and western Nevada. U.S. Geological Survey Professional Paper 623, 42.

Felzer, K.R., Beroza, G.C., 1999. Deep structure of a fault discontinuity. Geophysical Research Letters 26, 2121–2124.

Gillespie, P.A., Walsh, J.J., Watterson, J., 1992. Limitations of dimension and displacement data from single faults and the consequences for data analysis and interpretation. Journal of Structural Geology 14, 1157–1172.

Grannier, T., 1985. Origin, damping, and pattern of development of faults in granite. Tectonics 4, 721–737.

Green, D.C., Schweickert, R.A., 1995. The Gem Lake shear zone: Cretaceous dextral transpression in the northern Ritter Range pendant, eastern Sierra Nevada, California. Tectonics 14, 945–961.

Guatteri, M., Spudich, P., 1998. Coseimic temporal changes of slip direction: the effect of absolute stress on dynamic rupture. Bulletin of the Seismological Society of America 88, 777–789.

Gupta, A., Scholz, C.H., 2000. A model of normal fault interaction based on observations and theory. Journal of Structural Geology 22, 865–879.

Harris, R.A., Day, S.M., 1993. Dynamics of fault interaction: parallel strike-slip faults. Journal of Geophysical Research 98, 4461–4472.

Harris, R.A., Day, S.M., 1997. Effects of a low-velocity zone on dynamic rupture. Bulletin of the Seismological Society of America 87, 1267–1280.

Harris, R.A., Day, S.M., 1999. Dynamic 3D simulations on earthquakes on en échelon faults. Geophysical Research Letters 26, 2089–2092.

Hough, S.E., Ben-Zion, Y., Leary, P., 1994. Fault-zone waves observed at the southern Joshua Tree earthquake rupture zone. Bulletin of the Seismological Society of America 84, 761–767.

Lockwood, J.P., Lydon, P.A., 1975. Geologic map of the Mount Abbot quadrangle, central Sierra Nevada, California. U.S. Geological Survey Geologic Quadrangle Map GQ-1155.

Lockwood, J.P., Moore, J.G., 1979. Regional deformation of the Sierra Nevada, California, on conjugate microfault sets. Journal of Geophysical Research 84, 6041–6049.

Martel, S.J., 1990. Formation of compound strike-slip fault zones, Mount Abbot quadrangle, California. Journal of Structural Geology 12, 869–882.

Martel, S.J., 1999. Mechanical controls on fault geometry. Journal of Structural Geology 21, 585–596.

Martel, S.J., Boger, W.A., 1998. Geometry and mechanics of secondary fracturing around small three-dimensional faults in granitic rock. Journal of Geophysical Research 103, 21,299–21,314.

Martel, S.J., Pollard, D.D., 1989. Mechanics of slip and fracture along small faults and simple strike-slip fault zones in granitic rock. Journal of Geophysical Research 94, 9417–9428.

Martel, S.J., Pollard, D.D., Segall, P., 1988. Development of simple strike-slip fault zones, Mount Abbot quadrangle, Sierra Nevada, California. Geological Society of America Bulletin 100, 1451–1465.

Martel, S.J., Burgmann, R., Pollard, D.D., 1990. Ductile deformation associated with brittle faulting in granitic rock, Sierra Nevada, California. American Geophysical Union Transactions 71, 1558.

McGrath, A., Davidson, I., 1995. Damage zone geometry around fault tips. Journal of Structural Geology 17, 1011–1124.

Moore, D.E., Lockner, D.A., 1995. The role of microcracking in shear-fracture propagation in granite. Journal of Structural Geology 17, 95–114.

Passchier, C.W., Trouw, R.J., 1996. Microtectonics. Springer, Berlin.

Peacock, D.C.P., Sanderson, D.J., 1991. Displacements, segment linkage and relay ramps in normal fault zones. Journal of Structural Geology 13, 721–733.

Peacock, D.C.P., Sanderson, D.J., 1994. Geometry and development of relay ramps in normal fault systems. American Association of Petroleum Geologists Bulletin 78, 147–165.

Reches, Z., Lockner, D.A., 1994. Nucleation and growth of faults in brittle rocks. Journal of Geophysical Research 99, 18159–18173.

Roberts, G.P., 1996. Variation in fault-slip directions along active and segmented normal fault systems. Journal of Structural Geology 18, 835–845.

Robeson, K.R., 1998. Three-dimensional structure of small strike-slip fault zones in granitic rock: implications for fault growth models. M.S. thesis, Utah State University.

Rubin, A.M., Gillard, D., Got, J.-L., 1999. Streaks of microearthquakes along creeping faults. Nature 400, 635–641.

Schulz, S.E., Evans, J.P., 1998. Spatial variability in microscopic deformation and composition of the Punchbowl fault, southern California: implications for mechanisms, fluid-rock interactions, and fault morphology. Tectonophysics 295, 223–244.

Segall, P., Pollard, D.D., 1983a. Joint formation in granitic rock of the Sierra Nevada. Geological Society of America Bulletin 94, 563–575.

Segall, P., Pollard, D.D., 1983b. Nucleation and growth of strike slip faults in granite. Journal of Geophysical Research 88, 555–568.

Segall, P., Mckee, E.H., Martel, S.J., Turrin, B.D., 1990. Late Cretaceous age of fractures in the Sierra Nevada batholith, California. Geology 18, 1248–1251.

Shipton, Z.K., Cowie, P.A., 2001. Damage zone and slip-surface evolution over μm to km scales in high porosity Navajo sandstone, Utah. Journal of Structural Geology 23, 1825–1844.

Spudich, P., Guatteri, M., Otsuki, K., Minagawa, J., 1998. Use of fault striations and dislocation models to infer tectonic shear stress during the 1995 Hyogo-ken Nanbu (Kobe) earthquake. Bulletin of the Seismological Society of America 88, 413–427.

Sylvester, A.G., 1988. Strike-slip faults. Geological Society of America Bulletin 100, 1666–1703.

Tchalenko, J.S., Abraseys, N.N., 1970. Structural analysis of the Dasht-e Bayaz (Iran) earthquake fractures. Geological Society of America Bulltin 81, 41–60.

Tikoff, B., 1994. Transpression: strain theory and application to the emplacement and deformation of granite, Sierra Nevada, California. Ph.D. thesis, University of Minnesota.

Tikoff, B., Greene, D., 1994. Transpressional deformation within the Sierra Crest shear zone system, Sierra Nevada, California (92–80 Ma): vertical and horizontal stretching lineations within a single shear zone. Geological Society of America Abstracts with Programs 26, 385.

Tikoff, B., Saint Blanquat, M., 1997. Transpressional shearing and strike-slip partitioning in the Late Cretaceous Sierra Nevada magmatic arc. California. Tectonics 16, 442–459.

Wald, D., Helmberger, D.V., Heaton, T.H., 1991. Rupture model of the 1989 Loma Prieta earthquake from the inversion of strong motion and broadband teleseismic data. Bulletin of the Seismological Society of America 81, 1540–1572.

Walsh, J.J., Watterson, J., 1991. Geometric and kinematic coherence and scale effects in normal fault systems. In: Roberts, A.M., Yielding, G., Freeman, B. (Eds.), The Geometry of Normal Faults. Special Publications of the Geological Society of London 56, pp. 193–203.

Wesnousky, S.G., 1986. Earthquakes, quaternary faults, and seismic hazard in California. Journal of Geophysical Research 91, 12587–12631.

Wibberley, C.A.J., Petit, J.-P., Rives, T., 2000. Micromechanics of shear rupture and the control of normal stress. Journal of Structural Geology 22, 411–427.

Willemse, E.J.M., Pollard, D.D., Aydin, A., 1996. Three-dimensional analyses of slip distribution on normal fault arrays with consequences for fault scaling. Journal of Structural Geology 18, 295–309.